JOURNAL OF GUIDANCE, CONTROL, AND DYNAMICS
Vol. 45, No. 11, November 2022

Cascaded Lyapunov Vector Fields for Acceleration-Constrained Spacecraft Path Planning

Jeffrey Hough* and Steve Ulrich†
Carleton University, Ottawa, Ontario K1S 5B6, Canada

https://doi.org/10.2514/1.G006260

A variant of Lyapunov vector fields is presented for tracking trajectories within tumbling and accelerating reference frames. This extension is computationally light, and is acceleration constrained rather than velocity constrained, making it suitable for real-time use in spacecraft. A general stability analysis proves globally asymptotic stability given a set of conditions that are analogous to those of standard Lyapunov vector fields. A special case of this novel path-planning law (referred to as a cascaded Lyapunov vector field) is closely studied, and a simple set of conditions guaranteeing bounded acceleration commands for perfect tracking are derived. A design procedure is presented. Finally, a full design example for a spacecraft proximity inspection mission is presented. The simulations demonstrate stable behavior while respecting acceleration and path constraints. Furthermore, all constraints are met by judicious design of the path-planning field, without the need for computationally expensive algorithms running in real-time.

I. Introduction

IN RECENT years, autonomous flight algorithms have become an increasingly popular area of research. Driven by factors such as the development of unmanned aerial vehicles (UAVs) and increasing autonomy needs for spacecraft, these algorithms span high-level decision making, path planning, state estimation, low-level flight control, and many other topics. At a minimum, any well-designed autonomous algorithm will meet performance requirements while respecting the physical capabilities of the controlled vehicle. To meet these constraints, control designers often make use of optimization in-the-loop type algorithms such as model predictive control (MPC) [1–5] or inverse dynamics-based trajectory planning [6]. However, as is well-discussed in [7], computational load is a significant challenge when implementing algorithms such as on-board spacecraft in real-time. Methods with lighter computational requirements are usually not naturally equipped to handle constraints.

In this context, one computationally simple yet effective path-planning method that has arisen for UAVs is the kinematics-based *Lyapunov vector field* (LVF). As is well known, the typical use for a Lyapunov function is to prove the stability of a given system. Lyapunov vector fields, however, invert this process, and instead begin with a desirable Lyapunov function, and then use its properties to create guidance and control laws that are inherently asymptotically stable. Generally, LVFs map each given position in space to a desired velocity. Therefore, constraints such as velocity or curvature limitations can be addressed directly by judicious design of this mapping. Furthermore, path constraints can be directly addressed by shaping the LVF to avoid undesirable regions. For example, Hough and Ulrich [7] and Scorsoglio and Furfaro [8] defined path constraints within LVFs to avoid misalignment during spacecraft docking.

Lawrence [9] first introduced LVFs for standoff stationary-target tracking, and a general mathematical construct for deriving simple three-dimensional position-based LVFs for stand-off tracking was later presented by Lawrence et al. [10]. Beyond this general construction, Lawrence et al. [10] also presented some expanded LVF capabilities compared to previous applications, such as the ability to track "warped-circular" patterns, and a switching algorithm for waypoint path planning. This work was then expanded upon by Frew et al. [11] for two UAVs performing phase-shifted cooperative stand-off tracking of a moving ground vehicle with perturbations from wind.

Several authors have studied how [9–11] can be altered to bound the flight paths curvature. For example, Pothen and Ratnoo [12] proposed a curvature parameter that is a function of radial distance, causing a more direct path with bounded curvature characteristics both inside and outside of the stand-off radius. Extending upon [12], Sun et al. [13] proposed a set of more complex parameters, and performed an offline search to numerically select the curvature parameter, which minimized convergence time without violating the maximum turn rate. Very recent work by Che et al. [14] has further studied cooperative standoff tracking of moving targets (similar to the problem studied in [11]) in combination with curvature analysis. Specifically, the authors focused on optimizing the curvature parameter for minimum convergence time with a different algorithm compared to [13]. Moreover, Che et al. [14] better defined the target state-estimation subsystem of the UAV flock, and an interacting multiple model-based unscented Kalman filter was proposed. While UAV standoff tracking has been studied extensively, some authors have expanded LVFs beyond this application. For example, LVFs and other related vector fields have been proposed for UAV obstacle avoidance [15,16].

More recently, LVFs have been recognized as an attractive method for spacecraft, due to the ability to handle constraints with little computational load [7,8]. However, this change of application has required significant alterations to the existing literature. For example, all works relating to UAV applications have been subject to a constant (or nearly constant) inertial velocity constraint for remaining in steady flight. With spacecraft maneuvers, however, maintaining a constant velocity becomes unnecessary, and in fact impractical. One obvious example is that of docking, where desired relative velocity between the controlled spacecraft and uncontrolled target should converge to zero upon contact. Indeed, rather than being constrained by velocity, spacecraft are limited by their acceleration. The most important distinction, however, is the requirement of spacecraft to track trajectories that are defined with respect to rotating or tumbling reference frames. This requirement significantly complicates respecting the spacecraft acceleration constraints, as the acceleration experienced from the rotation of the trajectory must also be compensated.

Scorsoglio and Furfaro [8] used an LVF-based relative motion guidance for docking in a cislunar space environment. Quite uniquely, Scorsoglio and Furfaro [8] use an extreme learning machine (ELM) approach, such that the controlled spacecraft learns an LVF that can perform docking while meeting thrust constraints and

Received 7 June 2021; revision received 25 May 2022; accepted for publication 15 August 2022; published online 6 October 2022.

*M.A.Sc., Graduate Research Assistant, Department of Mechanical and Aerospace Engineering, 1125 Colonel By Drive.

†Associate Professor, Department of Mechanical and Aerospace Engineering, 1125 Colonel By Drive. Senior Member AIAA.

avoiding obstacles. Because an artificial intelligence approach is taken, the authors are also able to include fuel optimizations, which is not conventionally considered with LVFs. One important assumption used in [8], however, is that the target spacecraft is well-controlled, and therefore has a constant attitude with reference to a slowly rotating orbital reference frame. To compensate for the rotation of this reference frame without violating thrust constraints, the authors include the slowly evolving nonlinear dynamics equations directly in their training. However, it is unclear whether this method of training thrust limitation by inclusion of known reference-frame dynamics can be extended to include the tumbling of a spacecraft with arbitrary inertial properties and initial conditions.

In previous work by Hough and Ulrich [7], a different approach is taken to the docking problem by developing an LVF for a tumbling target based on body-fixed coordinates. The two spacecraft are assumed to be in nearly identical orbits when the docking procedure initializes, and therefore the acceleration differences due to gravity are considered negligible compared to the control inputs. It is assumed that the chaser spacecraft can obtain basic information about the target through observation, such as the maximum angular velocity and angular acceleration norms. Through a classical Lyapunov construction, asymptotic stability is guaranteed to the docking port. A maximum relative velocity and a radius of application are solved such that, when distance to the docking port is less than the radius of application, the trajectory combined with compensation of the rotating reference frame cannot exceed the chaser thrust limitations. Outside this radius, the chaser simply ignores the attitude of the target and contracts inward at constant speed. Clearly, the behavior inside and outside of the radius of application represent two different path-planning modes. However, there does not presently exist any obvious method to transition between these two modes while still meeting acceleration constraints and guaranteeing stability. Of course, such transitional trajectories are already possible to generate and track using some of the methods previously mentioned (MPC and inverse-dynamics based trajectory planning are both well-capable). However, to the authors' knowledge there do not exist any well-analyzed methods specifically designed for low computational power. Such work certainly does not presently exist in the framework of Lyapunov vector fields.

In this work, a variant to LVFs is introduced, herein referred to as a *cascaded Lyapunov vector field* (CLVF). In particular, this work extends LVFs to the case where the final desired trajectory is defined in a generally tumbling and accelerating reference frame, and the controlled vehicle is subject to acceleration constraints rather than velocity constraints. The CLVF is therefore significantly more applicable to spacecraft applications compared to conventional LVFs.

The remainder of this work is organized as follows: Sec. II reviews necessary theory from existing LVF literature. Then, Sec. III introduces the vector notation used in this work, and gives the problem formulation for this work. The general structure of CLVFs is then introduced in Sec. IV, and global asymptotic stability is proven, given a new set of conditions analogous to those required for standard LVFs. Conditions under which the required tracking acceleration is bounded are also derived in Sec. IV. Section V proposes a design procedure for the CLVF, and provides a design example for a spacecraft inspection mission. After performing the design, the CLVF performance is analyzed for several different acceleration constraints. Finally, Sec. VI presents the conclusions.

II. Review of Lyapunov Vector Field Theory

For completeness, this section reviews the theory and use of LVFs to date. Specifically, Sec. II.A will review the fundamental-level theory of LVFs, based on [10]. Section II.B will then review a design case for a UAV performing stand-off tracking on a stationary target. This review is designed to familiarize the reader with LVFs and is not intended to be comprehensive beyond what is necessary for further developments. Further details can be found in [9,11–16] and the works referenced therein.

A. General Lyapunov Vector Field Theory

Consider a dynamic closed-loop system

$$\dot{\boldsymbol{x}} = f(\boldsymbol{x}) \tag{1}$$

where $\boldsymbol{x} \in \mathbb{R}^n$ is a state vector. Additionally, design a Lyapunov function of the states given by $V(\boldsymbol{x}) \in \mathbb{R}$, where it is required that $V \geq 0$. An *attractor* $\mathbb{A} \subset \mathbb{R}^n$ is defined as the set $\mathbb{A} = \{\boldsymbol{x} | V(\boldsymbol{x}) = 0\}$. To prove globally asymptotically stable guidance, there are four conditions of the Lyapunov function V [10]:

A1) $V(\mathbb{A}) = 0$; otherwise $V(\boldsymbol{x}) > 0$.

A2) V is radially unbounded; as $\|\boldsymbol{x}\| \to \infty$, $V \to \infty$.

A3) V is continuously differentiable, and $\partial V/\partial \boldsymbol{x}$ is only $\boldsymbol{0}$ within $\mathbb{A}$.

A4) V is solely a function of $\boldsymbol{x}$ (i.e., not an explicit function of time).

The LVF $\boldsymbol{h}(\boldsymbol{x})$ is then given as the sum of two components:

$$\boldsymbol{h}(\boldsymbol{x}) = \boldsymbol{c}(\boldsymbol{x}) + \boldsymbol{s}(\boldsymbol{x}) \tag{2}$$

where $\boldsymbol{c}(\boldsymbol{x})$: $\mathbb{R}^n \to \mathbb{R}^n$ always points toward the attractor, and $\boldsymbol{s}(\boldsymbol{x})$:$\mathbb{R}^n \to \mathbb{R}^n$ is always perpendicular to the gradient of V. That is, the following conditions must be met:

B1)

$$\boldsymbol{c}(\boldsymbol{x}) = -\boldsymbol{\Gamma}(\boldsymbol{x})\frac{\partial V^T}{\partial \boldsymbol{x}}$$

B2)

$$\frac{\partial V}{\partial \boldsymbol{x}}\boldsymbol{s}(\boldsymbol{x}) = 0$$

where $\boldsymbol{\Gamma}(\boldsymbol{x}) \in \mathbb{R}^{n\times n}$ is a positive definite matrix with respect to the set $\mathbb{A}$. That is, $\boldsymbol{\Gamma}(\boldsymbol{x}, \cdot)$ is symmetric, and the quadratic product

$$q = (\boldsymbol{x} - \mathbb{A})^T\boldsymbol{\Gamma}(\boldsymbol{x})(\boldsymbol{x} - \mathbb{A}) \tag{3}$$

is positive everywhere, except for when $\boldsymbol{x} \in \mathbb{A}$, where $q = 0$. In this product, $(\boldsymbol{x} - \mathbb{A})$ is used to represent the shortest vector connecting the attractor $\mathbb{A}$ to the point $\boldsymbol{x}$. Almost invariantly, $\boldsymbol{\Gamma}(\boldsymbol{x})$ is the identity matrix multiplied by a positive-definite scalar function. Asymptotic stability of $\boldsymbol{x}$ to the set $\mathbb{A}$ can then be guaranteed by the following straightforward proof, given in several of the references [10,12].

Theorem 1: Assuming perfect tracking of the LVF guidance given by Eq. (2) and constraints A1–A4, B1, and B2, the state vector $\boldsymbol{x}$ is globally asymptotically stable to the set $\mathbb{A}$.

Proof 1: Given condition A4, the time derivative of V is found by

$$\dot{V} = \frac{\partial V}{\partial \boldsymbol{x}}\dot{\boldsymbol{x}} \tag{4}$$

By assuming perfect tracking of the trajectory described by the LVF,

$$\dot{V} = \frac{\partial V}{\partial \boldsymbol{x}}(\boldsymbol{c}(\boldsymbol{x}) + \boldsymbol{s}(\boldsymbol{x})) \tag{5}$$

Using constraints B1 and B2, this simplifies to

$$\dot{V} = -\frac{\partial V}{\partial \boldsymbol{x}}\boldsymbol{\Gamma}(\boldsymbol{x})\frac{\partial V^T}{\partial \boldsymbol{x}} \tag{6}$$

Constraints A1–A3 then complete the proof. □

Note that because LVFs are path planners, some control method is required to track the desired path. The following acceleration controller is proposed by Lawrence et al. [10]:

$$\ddot{\boldsymbol{x}}(\boldsymbol{x}, \boldsymbol{h}) = -\beta(\dot{\boldsymbol{x}} - \boldsymbol{h}) + \dot{\boldsymbol{h}} \tag{7}$$

where $\beta \in \mathbb{R}$ is a strictly positive parameter. Asymptotic tracking of the LVF is then given by the following:

Theorem 2: Under the acceleration law given by Eq. (7), the time derivative of the controlled states, $\dot{\boldsymbol{x}}$, is globally asymptotically convergent to the LVF, $\boldsymbol{h}(\boldsymbol{x})$.

Proof 2: To begin, we define an error Lyapunov function W as

$$W = \frac{(\dot{\boldsymbol{x}} - \boldsymbol{h})^T(\dot{\boldsymbol{x}} - \boldsymbol{h})}{2} \tag{8}$$

which clearly meets A1–A4, where tracking error is the state. A time derivative of W then results in

$$\dot{W} = (\dot{\boldsymbol{x}} - \boldsymbol{h})^T(\ddot{\boldsymbol{x}} - \dot{\boldsymbol{h}}) \tag{9}$$

and substitution of Eq. (7) results in

$$\dot{W} = -\beta(\dot{\boldsymbol{x}} - \boldsymbol{h})^T(\dot{\boldsymbol{x}} - \boldsymbol{h}) \tag{10}$$

which completes the proof. □

B. Lyapunov Vector Fields for Unmanned Air Vehicles

Let us now present a design example for UAV standoff tracking of a stationary target, based on [10]. To begin, define a vector $\hat{\boldsymbol{n}} \in \mathbb{R}^3$ that is normal to the desired circular trajectory. Further, the controlled state is selected as the position vector $\boldsymbol{r} \in \mathbb{R}^3$, and $\boldsymbol{r} = \boldsymbol{0}$ is defined to be directly above the target at the desired altitude. The next step is to select a Lyapunov function on which to construct the LVF. One option is [10]

$$V(\boldsymbol{r}) = \frac{1}{2}(\boldsymbol{r}_n^T\hat{\boldsymbol{r}}_n)^2 + \frac{1}{2}(\boldsymbol{r}_t^T\hat{\boldsymbol{r}}_t - \eta)^2 \tag{11}$$

where $\eta \in \mathbb{R} > 0$ is the desired circular radius, $\hat{\{\cdot\}}$ denotes a vector of unit magnitude in the direction of $\{\cdot\}$, and subscripts t and n denote the tangent and normal components with reference to the normal vector $\hat{\boldsymbol{n}}$. That is,

$$\boldsymbol{r}_n = \hat{\boldsymbol{n}}\hat{\boldsymbol{n}}^T\boldsymbol{r} \tag{12}$$

$$\boldsymbol{r}_t = (\boldsymbol{I} - \hat{\boldsymbol{n}}\hat{\boldsymbol{n}}^T)\boldsymbol{r} \tag{13}$$

where, throughout this work, $\boldsymbol{I}$ will refer to the identity matrix of appropriate dimension. Note that $V = 0$ if and only if $r_n = 0$ and $r_t = \eta$, defining the attractor $\mathbb{A}$ (it will be common notation to use nonbold letters to refer to norms, i.e., $r_n = \|\boldsymbol{r}_n\|$ and $r_t = \|\boldsymbol{r}_t\|$). Analyzing Eq. (11), it is clear that the conditions A1–A4 are met. Equation (11) can be used to build the following path-planning law:

$$\boldsymbol{h}(\boldsymbol{r}) = -\boldsymbol{\Gamma}(\boldsymbol{r})\frac{\partial V^T}{\partial \boldsymbol{r}} + \boldsymbol{s}(\boldsymbol{r}) \tag{14}$$

where $\boldsymbol{h}(\boldsymbol{r})$ is the desired velocity, $\boldsymbol{\Gamma}(\boldsymbol{r})$ is positive definite (and usually a multiple of the identity) matrix, and $\boldsymbol{s}(\boldsymbol{r})$ is the *circulation* term, as it will cause the UAV to fly in a circle upon arrival to the attractor. Options for $\boldsymbol{\Gamma}(\boldsymbol{r})$ and $\boldsymbol{s}(\boldsymbol{r})$ that keep the UAV flying at a constant speed are

$$\boldsymbol{\Gamma}(\boldsymbol{r}) = \frac{1}{\alpha(\boldsymbol{r})}\boldsymbol{I} \tag{15}$$

$$\boldsymbol{s}(\boldsymbol{r}) = \gamma\frac{\hat{\boldsymbol{n}}^{\times}\boldsymbol{r}_t}{\alpha(\boldsymbol{r})} \tag{16}$$

where $\gamma \in \mathbb{R}$ denotes a curvature parameter (well-studied in [12–14]), $\{\cdot\}^{\times}$ denotes the skew-symmetric construction of $\{\cdot\}$ used for computing cross-products, and α is a normalization parameter given by

$$\alpha(\boldsymbol{r}) = \frac{1}{v}(r_n^2 + (r_t - \eta)^2 + r_t^2\gamma^2)^{1/2} \tag{17}$$

where $v \in \mathbb{R} > 0$ is the constant desired speed. By shifting parameters such as γ or v, various "shapes" of LVF can be formed, resulting in varying trajectories toward and around the desired circle of radius η as seen in Fig. 1.

III. Problem Formulation

Section III.A introduces the notation used for the remainder of this work. Then, Sec. III.B provides motivation for why the present LVF theory is not well suited for generally rotating and translating reference frames, and defines the desired characteristics of the proposed variant.

A. Reference Frame and Vector Definitions

To begin, let us define a body-fixed reference frame B that is fixed to the target position and orientation, and an inertial reference frame I. The origin of B relative to the origin of I is given by the vector $\boldsymbol{d}(t) \in \mathbb{R}^3$. The controlled vehicle position relative to the origin of I is denoted $\boldsymbol{r}_w(t) \in \mathbb{R}^3$, and relative to the origin of B is denoted $\boldsymbol{r}(t) \in \mathbb{R}^3$. The rotation matrix that converts B coordinates into I coordinates is given by $\boldsymbol{C}_{IB}(t) \in \mathbb{R}^{3\times3}$. Finally, the angular velocity of B relative to I is exactly equal to the angular velocity of the rigid target, denoted $\boldsymbol{\omega}_{BI}(t)$. There is an attractor $\mathbb{A}_c$ that is stationary when viewed from B. The desired position within the attractor is described

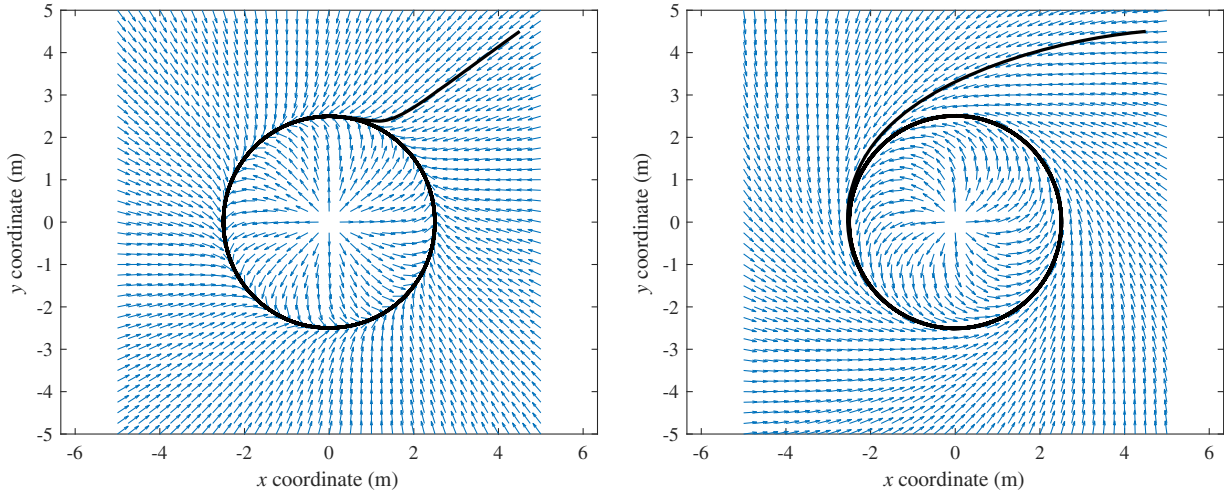

a) Lyapunov vector field with $\gamma = 0.1$ **b) Lyapunov vector field with $\gamma = 0.5$**

Fig. 1 Lyapunov vector fields with $\eta = 3$, $\hat{n}$ in z direction.

by the time-varying vector $\boldsymbol{o}(t) \in \mathbb{R}^3$ that, by definition, must have a magnitude such that the tip of the vector is on the surface $\mathbb{A}_c$. Lastly, let us define the angle between $\boldsymbol{r}(t)$ and $\boldsymbol{o}(t)$ as $\theta(t)$. A diagram of these definitions is given in Fig. 2.

Note that for the remainder of this paper, the argument of time will typically be omitted. Furthermore, when expressing vectors in a noninertial reference frame, a superscript will denote the reference frame being used.

B. Tracking Lyapunov Vector Fields in Rotating Reference Frames

Suppose that the controlled vehicle has some desired trajectory defined in B. If LVFs are to be used, then the attractor $\mathbb{A}_c$ must be defined as a constant set of coordinates in B, and the desired trajectory must move through $\mathbb{A}_c$. If $\boldsymbol{\omega}_{BI}$ is slow enough, it may be reasonable to define the LVF directly in B. That is, the guidance would be defined as

$$\boldsymbol{h}^B = \boldsymbol{c}^B(\boldsymbol{r}^B) + \boldsymbol{s}^B(\boldsymbol{r}^B) \tag{18}$$

The required acceleration to track this field is then given as

$$\dot{\boldsymbol{h}} = \ddot{\boldsymbol{d}} + \boldsymbol{C}_{IB}(\boldsymbol{\omega}_{BI}^{\times}\boldsymbol{\omega}_{BI}^{\times}\boldsymbol{r}^B + \dot{\boldsymbol{\omega}}_{BI}^{\times}\boldsymbol{r}^B + 2\boldsymbol{\omega}_{BI}^{\times}\boldsymbol{h}^B + \dot{\boldsymbol{h}}^B) \tag{19}$$

Immediately, there is the issue that as $\|\boldsymbol{r}\| \to \infty$, $\|\dot{\boldsymbol{h}}\| \to \infty$ provided that $\boldsymbol{\omega}_{BI} \neq \boldsymbol{0}$ and that $\boldsymbol{\omega}_{BI}$ is not perfectly parallel to $\boldsymbol{r}$. Unless the target rotation is assumed to be very slow, as is the case in [8], tracking this LVF will quickly saturate thrusters. Therefore, simply taking the existing LVF framework and applying it within a tumbling reference frame in an ad-hoc manner is not a good solution.

In this paper, the authors propose a variant of the LVF, herein referred to as the cascaded Lyapunov vector field (CLVF). The purpose of this variant is to suitably adjust the existing LVF framework for use in spacecraft. That is, the resulting field should consider the maximum acceleration constraints, and the field should naturally apply when the final desired trajectory is defined in a tumbling reference frame. Furthermore, the very attractive quality of simplicity, characteristic of the LVF framework, should be preserved as much as possible.

IV. Cascaded Lyapunov Vector Fields

A. Structure

To begin, let us define a Lyapunov function V_c that meets A1–A4 for the state $\boldsymbol{r}$. The CLVF is given the familiar high-level structure:

$$\boldsymbol{h}(\boldsymbol{r}) = \boldsymbol{c}(\boldsymbol{r}) + \boldsymbol{s}(\boldsymbol{r}) + \dot{\boldsymbol{d}} \tag{20}$$

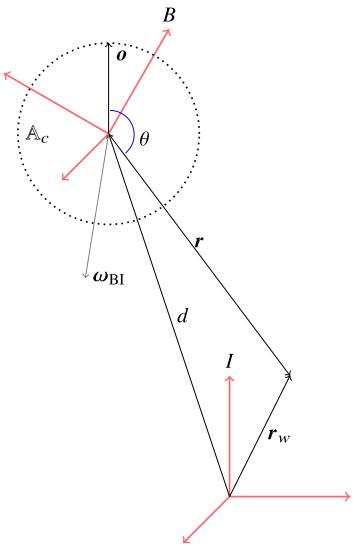

Fig. 2 Reference frame and vector definitions.

where $\dot{\boldsymbol{d}}$ is the time derivative of the target position, $\boldsymbol{c}(\boldsymbol{r})$ has the structure

$$\boldsymbol{c}(\boldsymbol{r}) = -\boldsymbol{\Gamma}_c(\boldsymbol{r})\frac{\partial V_c^T}{\partial \boldsymbol{r}} \tag{21}$$

and $\boldsymbol{s}(\boldsymbol{r})$ is subject to B2 for the Lyapunov function V_c. Therefore, the CLVF *is* in fact an LVF, and inherits the globally asymptotic stability properties to the attractor $\mathbb{A}_c$. Let us depart from standard LVFs by defining a desired trajectory within $\mathbb{A}_c$ and provide the term $\boldsymbol{s}(\boldsymbol{r})$ with the following structure:

$$\boldsymbol{s}(\boldsymbol{r}, \boldsymbol{o}) = \boldsymbol{a}(\boldsymbol{r}, \boldsymbol{o}) + \boldsymbol{g}(\boldsymbol{r}, \dot{\boldsymbol{o}}) \tag{22}$$

where $\boldsymbol{g}:\mathbb{R}^3 \times \mathbb{R}^3 \to \mathbb{R}^3$ is a velocity function responsible for tracking the attitude of the reference frame B, and $\boldsymbol{a}:\mathbb{R}^3 \times \mathbb{R}^3 \to \mathbb{R}^3$ is a function referred to as the "alignment" component of velocity with the structure

$$\boldsymbol{a}(\boldsymbol{r}, \boldsymbol{o}) = -\boldsymbol{\Gamma}_a(\boldsymbol{r}, \boldsymbol{o})\frac{\partial V_a^T}{\partial \boldsymbol{r}} \tag{23}$$

where V_a is a Lyapunov function of θ meeting constraints A1, A3, and A4, and its attractor is the single desired trajectory point $\boldsymbol{o}(t)$. Note that V_a does not meet A2 as θ exists in a bounded set $[0, \pi]$ and therefore does not require global stability properties. The matrix $\boldsymbol{\Gamma}_a \in \mathbb{R}^{3\times3}$ is not necessarily positive definite, but must be positive semidefinite. In particular, $\boldsymbol{\Gamma}_a(\boldsymbol{r}, \boldsymbol{o})$ can have a nontrivial null space anytime $\boldsymbol{r}$ and $\boldsymbol{o}$ are parallel or antiparallel. Lastly, let us mandate the following property for $\boldsymbol{g}(\boldsymbol{r}, \dot{\boldsymbol{o}})$:

$$\frac{\partial V_a}{\partial \boldsymbol{r}}\boldsymbol{g}(\boldsymbol{r}, \dot{\boldsymbol{o}})|_{r\in\mathbb{A}_c} = -\frac{\partial V_a}{\partial \boldsymbol{o}}\dot{\boldsymbol{o}} \tag{24}$$

The resulting path planner is therefore an LVF with a second LVF-like structure embedded in the $\boldsymbol{s}(\boldsymbol{r}, \boldsymbol{o})$ term, meant to converge a spacecraft to a specific trajectory defined inside of the attractor $\mathbb{A}_c$.

B. Stability

Note that stability of $\boldsymbol{r}$ to the attractor $\mathbb{A}_c$ following the path-planner Eq. (20) follows directly from Theorem 1. What is left, therefore, is to prove asymptotic stability to the trajectory-tracking point $\theta = 0$.

Theorem 3: Assuming perfect tracking to the CLVF guidance given by Eq. (20), the vector $\boldsymbol{r}$ is asymptotically stable to the point $\boldsymbol{o}(t)$, which is the attractor for a Lyapunov function V_a meeting A1, A3, and A4 for the state θ.

Proof 3: Taking the time derivative of V_a gives

$$\dot{V}_a = \frac{dV_a}{d\theta}\dot{\theta} \tag{25}$$

or equivalently, using the fact that θ is a function of $\boldsymbol{r}$ and $\boldsymbol{o}$

$$\dot{V}_a = \frac{\partial V_a}{\partial \boldsymbol{r}}\dot{\boldsymbol{r}} + \frac{\partial V_a}{\partial \boldsymbol{o}}\dot{\boldsymbol{o}} \tag{26}$$

Assuming perfect tracking, this leads to the expression

$$\dot{V}_a = \frac{\partial V_a}{\partial \boldsymbol{r}}(\boldsymbol{c}(\boldsymbol{r}) + \boldsymbol{a}(\boldsymbol{r}, \boldsymbol{o}) + \boldsymbol{g}(\boldsymbol{r}, \dot{\boldsymbol{o}})) + \frac{\partial V_a}{\partial \boldsymbol{o}}\dot{\boldsymbol{o}} \tag{27}$$

Invoking the structure of $\boldsymbol{c}(\boldsymbol{r})$ and $\boldsymbol{a}(\boldsymbol{r}, \boldsymbol{o})$ leads to

$$\dot{V}_a = -\frac{\partial V_a}{\partial \boldsymbol{r}}\boldsymbol{\Gamma}_a(\boldsymbol{r}, \boldsymbol{o}, \cdot)\frac{\partial V_a}{\partial \boldsymbol{r}}^T + \delta(\boldsymbol{r}) \tag{28}$$

where $\delta(\boldsymbol{r})$ is a disturbance term given by

$$\delta(\boldsymbol{r}) = \left(\frac{\partial V_a}{\partial \boldsymbol{o}}\dot{\boldsymbol{o}} + \frac{\partial V_a}{\partial \boldsymbol{r}}\boldsymbol{g}(\boldsymbol{r},\dot{\boldsymbol{o}})\right) - \frac{\partial V_a}{\partial \boldsymbol{r}}\boldsymbol{\Gamma}_c(\boldsymbol{r})\frac{\partial V_c^T}{\partial \boldsymbol{r}} \tag{29}$$

note that *independently* of this proof, Theorem 1 mandates that $\boldsymbol{r} \to \mathbb{A}_c$. Also, noting Eq. (24) and the fact that $\partial V_c^T/\partial \boldsymbol{r} = \boldsymbol{0}$ on $\mathbb{A}_c$ yields

$$\delta(\mathbb{A}_c) = 0 \tag{30}$$

Further, given that $\boldsymbol{\Gamma}_a$ has a trivial null-space everywhere except $\theta = 0$ and $\theta = \pi$, it can be said that for any θ that does *not* equal 0 or π, there is a contour of V_c that will eventually be reached such that

$$\left\| \frac{\partial V_a}{\partial \boldsymbol{r}}\boldsymbol{\Gamma}_a(\boldsymbol{r},\boldsymbol{o},\cdot)\frac{\partial V_a^T}{\partial \boldsymbol{r}} \right\| > \|\delta(\boldsymbol{r})\| \tag{31}$$

because $\boldsymbol{r}$ will be sufficiently close to $\mathbb{A}_c$ and therefore $\delta(\boldsymbol{r})$ will be sufficiently close to 0. At this point, $\dot{V}_a$ will become negative, and therefore $\dot{V}_a$ becomes negative semidefinite in $\boldsymbol{r}$. To prove that $\dot{V}_a$ indeed becomes negative definite, let us show that $\partial V_a/\partial \boldsymbol{r}$ cannot become $\boldsymbol{0}$ anywhere except the points where $\theta = 0$ or $\theta = \pi$. First, given that V_a is a function of θ only, it is straightforward to solve the Jacobian $\partial V_a/\partial \boldsymbol{r}$ as

$$\frac{\partial V_a}{\partial \boldsymbol{r}} = \frac{dV_a}{d\theta}\frac{\partial \theta}{\partial \boldsymbol{r}} = \frac{dV_a}{d\theta}\left(\frac{\hat{\boldsymbol{r}}^T\cos\theta - \hat{\boldsymbol{o}}^T}{r\sin\theta}\right) \tag{32}$$

Setting this Jacobian to $\boldsymbol{0}$ and rearranging, the following condition arises:

$$\hat{\boldsymbol{r}}\cos\theta = \hat{\boldsymbol{o}} \tag{33}$$

which is impossible for any value of θ other than 0 or π. Noting that $\dot{V}_a(\theta) < 0$ everywhere within $\mathbb{A}_c$ except for these two points, it is clear that $\theta = \pi$ becomes an unstable equilibrium point because $V(\theta)$, and therefore θ will decrease away from π. By the same argument, $\theta = 0$ becomes an asymptotically stable equilibrium point as $\boldsymbol{r} \to \mathbb{A}_c$. □

C. Simplifying Assumptions

For the remainder of this work, a set of simplifying assumptions will be applied to the CLVF, which will ease the process of finding an upper acceleration bound. These assumptions are as follows:

C1) The attractor $\mathbb{A}_c$ is spherical with a radius $\alpha \in \mathbb{R} > 0$. The desired trajectory point can therefore be expressed as $\boldsymbol{o}(t) = \alpha\hat{\boldsymbol{o}}(t)$.

C2) The origin of the reference frame B is centered in the sphere $\mathbb{A}_c$.

C3) The matrices $\boldsymbol{\Gamma}_a(\boldsymbol{r},\boldsymbol{o})$ and $\boldsymbol{\Gamma}_c(\boldsymbol{r},\boldsymbol{o})$ are identity matrices multiplied by scalar functions.

C4) The function $\boldsymbol{g}(\boldsymbol{r},\dot{\boldsymbol{o}})$ is set such that $\boldsymbol{g}(\boldsymbol{r},\dot{\boldsymbol{o}}) = g(r,\theta)\omega_{OI}^{\times}\hat{\boldsymbol{r}}$, where $g(r,\theta)$:$\mathbb{R}\times\mathbb{R}\to\mathbb{R}$ is globally Lipschitz continuous in both arguments and is nonnegative, and $\boldsymbol{\omega}_{OI} \in \mathbb{R}^3$ is the angular velocity of the vector $\boldsymbol{o}$ with respect to the inertial frame I (the component of $\boldsymbol{\omega}_{OI}$ along $\boldsymbol{o}$ is always 0). Also, $g(r,\theta)$ is such that on the attractor $g(\alpha,\theta) = \alpha$.

C5) The function $V_c(\boldsymbol{r})$ is a function of distance to the attractor only. That is, $V_c(\boldsymbol{r}) = V_c(r)$

Note that each of the assumptions C1–C3 and C5 are almost universally applied in work pertaining to LVFs. Assumption C4 is just a specific form to meet the constraint given by Eq. (24), so long as $\mathbb{A}_c$ is spherical. The intuition for C4 is that on the attractor, $\boldsymbol{g}(\boldsymbol{r},\dot{\boldsymbol{o}}) = \omega_{OI}^{\times}\boldsymbol{r}$, which would exactly track the rotation of frame B.

Using C3, let us begin by rewriting these matrices in the form

$$\boldsymbol{\Gamma}_c(\boldsymbol{r}) = \frac{s_c(r,\theta)}{\|dV_c/d\boldsymbol{r}\|}\boldsymbol{I} \tag{34}$$

$$\boldsymbol{\Gamma}_a(\boldsymbol{r},\hat{\boldsymbol{o}}) = \frac{s_a(r,\theta)}{\|\partial V_a/\partial \boldsymbol{r}\|}\boldsymbol{I} \tag{35}$$

where $s_c(r,\theta)$ and $s_a(r,\theta)$ are yet-unselected speed functions that are globally Lipshcitz in both r and θ. For now, it is of no concern what the Lipschitz constant of either function is; this property is only important for constraining total CLVF acceleration. To meet positive definiteness, the function $s_c(r,\theta)$ is strictly positive, except on $\mathbb{A}_c$ where $s_c(\alpha,\theta) = 0$. Similarly, to meet the criteria on $\boldsymbol{\Gamma}_a(\boldsymbol{r},)$, $s_a(r,\theta)$ may be designed such that

$$\lim_{\theta\to 0} s_a(r,\theta) = \lim_{\theta\to\pi} s_a(r,\theta) = 0 \tag{36}$$

but is strictly positive otherwise. The CLVF can now be written in the form

$$\begin{aligned}\boldsymbol{h}(\boldsymbol{r},\boldsymbol{\omega}_{OI},\hat{\boldsymbol{o}},\dot{\boldsymbol{d}}) = {} & s_c(r,\theta)\hat{\boldsymbol{c}}(\boldsymbol{r}) + s_a(r,\theta)\hat{\boldsymbol{a}}(\hat{\boldsymbol{r}},\hat{\boldsymbol{o}}) \\ & + g(r,\theta)\boldsymbol{\omega}_{OI}^{\times}\hat{\boldsymbol{r}} + \dot{\boldsymbol{d}}\end{aligned} \tag{37}$$

where

$$\hat{\boldsymbol{c}} = -\frac{(\partial V_c/\partial \boldsymbol{r})^T}{\|\partial V_c/\partial \boldsymbol{r}\|} \tag{38}$$

$$\hat{\boldsymbol{a}} = -\frac{(\partial V_a/\partial \boldsymbol{r})^T}{\|\partial V_a/\partial \boldsymbol{r}\|} \tag{39}$$

Note that by using the assumption that V_c is a function of the distance from the attractor only, and setting $\hat{\boldsymbol{c}}$ to the null vector $\boldsymbol{0}$ when $\|\boldsymbol{r}\| = \alpha$ to avoid singularities in the solution, $\hat{\boldsymbol{c}}$ equates to

$$\hat{\boldsymbol{c}} = \begin{cases} -\hat{\boldsymbol{r}}, & \|\boldsymbol{r}\| > \alpha \\ \hat{\boldsymbol{r}}, & \|\boldsymbol{r}\| < \alpha \\ \boldsymbol{0}, & \text{otherwise} \end{cases} \tag{40}$$

Next, using the term $\partial\theta/\partial \boldsymbol{r}$ from Eq. (32), we note that

$$\left\|\frac{\partial \theta}{\partial \boldsymbol{r}}\right\| = \left(\frac{\partial \theta}{\partial \boldsymbol{r}}\frac{\partial \theta^T}{\partial \boldsymbol{r}}\right)^{1/2} = \frac{(1-\cos^2\theta)^{1/2}}{r\sin\theta} = \frac{1}{r} \tag{41}$$

such that $\hat{\boldsymbol{a}}$ can be defined as

$$\hat{\boldsymbol{a}} = -r\frac{\partial \theta^T}{\partial \boldsymbol{r}} \tag{42}$$

to have unity magnitude. To avoid singularities at $\theta = 0$ and $\theta = \pi$, $\hat{\boldsymbol{a}}$ can be therefore be computed as

$$\hat{\boldsymbol{a}} = \begin{cases} \dfrac{\hat{\boldsymbol{o}} - \hat{\boldsymbol{r}}\cos\theta}{\sin\theta}, & 0 < \theta < \pi, \\ \boldsymbol{0}, & \text{otherwise} \end{cases} \tag{43}$$

which also leads to the following useful relationship between $\hat{\boldsymbol{o}}$, $\hat{\boldsymbol{a}}$, and $\hat{\boldsymbol{r}}$:

$$\hat{\boldsymbol{o}} = \hat{\boldsymbol{r}}\cos\theta + \hat{\boldsymbol{a}}\sin\theta \tag{44}$$

Lastly, we rewrite the product $s_c(r,\theta)\hat{\boldsymbol{c}}$ as

$$s_c(r,\theta)\hat{\boldsymbol{c}} = v_c(r,\theta)\hat{\boldsymbol{r}} \tag{45}$$

where v_c is the contraction direction velocity function, as it encodes direction along the vector $\boldsymbol{r}$. That is,

$$v_c(r,\theta) = \begin{cases} s_c(r,\theta), & r < \alpha \\ -s_c(r,\theta), & \text{otherwise} \end{cases} \tag{46}$$

The main benefit of expressing the contraction velocity in this way is that we can then define a third unit vector

$$\hat{\boldsymbol{e}} = \hat{\boldsymbol{r}}^{\times}\hat{\boldsymbol{a}} \tag{47}$$

which will be useful in the acceleration analysis. If instead the vector $\hat{\boldsymbol{c}}$ were used to define $\hat{\boldsymbol{e}}$ with a cross-product, then the direction of $\hat{\boldsymbol{e}}$ would change whenever the sphere $r = \alpha$ was crossed. With this new unit vector $\hat{\boldsymbol{e}}$ being defined, it is useful to note that for every $\boldsymbol{r}$ except the line where $\theta = 0$ or $\theta = \pi$, the following identity holds:

$$\hat{\boldsymbol{r}}\hat{\boldsymbol{r}}^T + \hat{\boldsymbol{a}}\hat{\boldsymbol{a}}^T + \hat{\boldsymbol{e}}\hat{\boldsymbol{e}}^T = \boldsymbol{I} \tag{48}$$

The final special form of the CLVF to be used for analysis in the remainder of this work is then

$$\boldsymbol{h}(\boldsymbol{r}, \hat{\boldsymbol{o}}, \boldsymbol{\omega}_{OI}, \dot{\boldsymbol{d}}) = v_c(r,\theta)\hat{\boldsymbol{r}} + s_a(r,\theta)\hat{\boldsymbol{a}} + g(r,\theta)\boldsymbol{\omega}_{OI}^{\times}\hat{\boldsymbol{r}} + \dot{\boldsymbol{d}} \tag{49}$$

and the stability constraints placed on the more general CLVF can be translated to the following smaller set of conditions on $v_c(r,\theta)$, $s_a(r,\theta)$, and $g(r,\theta)$:
D1) $\operatorname{sgn}(v_c(r,\theta)) = \operatorname{sgn}(\alpha - r)$, and $v_c(\alpha,\theta) = 0$.
D2) $g(r,\theta) \geq 0$, and $g(\alpha,\theta) = \alpha$.
D3) It is allowed that $\lim_{\theta\to 0} s_a(r,\theta) = \lim_{\theta\to\pi} s_a(r,\theta) = 0$, but $s_a(r,\theta) > 0$ otherwise.

D. Upper Boundedness of the Required Tracking Acceleration

In the analysis that follows, we construct the necessary conditions on $v_c(r,\theta)$, $s_a(r,\theta)$, and $g(r,\theta)$ to guarantee that the CLVF bounds the acceleration required for tracking to some value $u_{\max} \in \mathbb{R} > 0$. For the time being, there is no concern as for exactly what value $u_{\max}$ is, but only that this bound exists. Later, a numerical CLVF parameter search will allow the user to select $u_{\max}$ to any feasible value.

Because only Lipschitz continuity (rather than continuous differentiability) is assumed, let us analyze a discrete change in the CLVF, assumed to have occurred over some finite period of time Δt.

$$\Delta\boldsymbol{h} = \Delta\boldsymbol{c} + \Delta\boldsymbol{a} + \Delta\boldsymbol{g} + \Delta\dot{\boldsymbol{d}} \tag{50}$$

Of course, *if* the acceleration magnitude is constrained by $u_{\max} \in \mathbb{R} > 0$, then by definition the CLVF is Lipschitz continuous in time such that

$$\|\Delta\boldsymbol{h}\| \leq u_{\max}\|\Delta t\| \tag{51}$$

is always true. The simplest way to ensure this condition is to mandate that each of the subfunctions $\boldsymbol{c}$, $\boldsymbol{a}$, $\boldsymbol{g}$, and $\dot{\boldsymbol{d}}$ are themselves Lipschitz continuous in time, which is the strategy employed here.

Assuming that $\boldsymbol{h}$ is Lipschitz continuous, there is a "weak" derivative of $\boldsymbol{h}$; that is, $\dot{\boldsymbol{h}}$ can be expressed as a bounded piecewise-continuous function made up of $K \in \mathbb{Z}$ continuous functions on their own time intervals (t_{i-1}, t_i), and that the discrete difference $\Delta\boldsymbol{h}$ can alternatively be expressed [17]

$$\Delta\boldsymbol{h} = \sum_{i=1}^{K}\int_{t_{i-1}}^{t_i}\dot{\boldsymbol{h}}\,\mathrm{d}t \tag{52}$$

where, for the remainder of this work, bounds will be dropped, with the understanding that $\sum\int\dot{\boldsymbol{h}}\,\mathrm{d}t$ represents the integral of a bounded piecewise-continuous function ($\dot{\boldsymbol{h}}$ in the example above) to form a bounded discrete step.

Let us therefore express the first term in Eq. (50) as

$$\Delta\boldsymbol{c} = \Delta(v_c(r,\theta)\hat{\boldsymbol{r}}) = \sum\int(\dot{v}_c(r,\theta)\hat{\boldsymbol{r}} + v_c(r,\theta)\dot{\hat{\boldsymbol{r}}})\,\mathrm{d}t \tag{53}$$

The time derivative $\dot{v}_c$ can be expressed (on the intervals where it is continuous) as

$$\dot{v}_c(r,\theta) = \frac{\partial v_c}{\partial r}\dot{r} + \frac{\partial v_c}{\partial\theta}\dot{\theta} \tag{54}$$

Because $v_c(r,\theta)$ is already assumed to be Lipschitz continuous in both r and θ, $\dot{v}_c(r,\theta)$ is bounded if $\dot{r}$ and $\dot{\theta}$ are bounded. When perfect tracking of the CLVF is assumed, the following expressions on the intervals of continuity for $\dot{r}$ and $\dot{\theta}$ can be derived:

$$\begin{aligned}\dot{r}|_{\dot{\boldsymbol{r}}=\boldsymbol{h}} &= \left.\frac{dr}{dt}\right|_{\dot{\boldsymbol{r}}=\boldsymbol{h}} = \frac{dr}{d\boldsymbol{r}}(\boldsymbol{h} - \dot{\boldsymbol{d}}) \\ &= \hat{\boldsymbol{r}}^T(v_c(r,\theta)\hat{\boldsymbol{r}} + s_a(r,\theta)\hat{\boldsymbol{a}} + g(r,\theta)\boldsymbol{\omega}_{OI}^{\times}\hat{\boldsymbol{r}}) = v_c(r,\theta)\end{aligned} \tag{55}$$

so $\dot{r}|_{\dot{\boldsymbol{r}}=\boldsymbol{h}}$ is bounded if $v_c(r,\theta)$ is bounded. Next, for $\dot{\theta}$

$$\begin{aligned}\dot{\theta}|_{\dot{\boldsymbol{r}}=\boldsymbol{h}} &= \left.\left(\frac{\partial\theta}{\partial\hat{\boldsymbol{r}}}\frac{d\hat{\boldsymbol{r}}}{d\boldsymbol{r}}\dot{\boldsymbol{r}} + \frac{\partial\theta}{\partial\hat{\boldsymbol{o}}}\dot{\hat{\boldsymbol{o}}}\right)\right|_{\dot{\boldsymbol{r}}=\boldsymbol{h}} = \left(\frac{-\hat{\boldsymbol{o}}^T}{\sin\theta}\right)\left(\frac{\boldsymbol{I} - \hat{\boldsymbol{r}}\hat{\boldsymbol{r}}^T}{r}\right)(v_c(r,\theta)\hat{\boldsymbol{r}} \\ &\quad + s_a(r,\theta)\hat{\boldsymbol{a}} + g(r,\theta)\boldsymbol{\omega}_{OI}^{\times}\hat{\boldsymbol{r}}) + \left(\frac{-\hat{\boldsymbol{r}}^T}{\sin\theta}\right)(\boldsymbol{\omega}_{OI}^{\times}\hat{\boldsymbol{o}}) \\ &= -\frac{s_a(r,\theta)}{r} + \left(1 - \frac{g(r,\theta)}{r}\right)\boldsymbol{\omega}_{OI}^T\hat{\boldsymbol{e}}\end{aligned} \tag{56}$$

where Eqs. (44), (47), and (48) have been used in the final step. Note the fact that Eq. (48) does not apply at $\theta = 0$ or $\theta = \pi$ is not of concern, as crossing one of these points causes discontinuities in the derivative, and therefore these points are excluded from the integrals of Eq. (54). Obviously, it is necessary that $\boldsymbol{\omega}_{OI}$ is bounded; otherwise it is impossible to track. Therefore $\dot{\boldsymbol{\theta}}|_{\dot{\boldsymbol{r}}=\boldsymbol{h}}$ is bounded if $s_a(r,\theta)/r$ and $g(r,\theta)/r$ are bounded. That is, if $r \to 0$, then it is required that $s_a(r,\theta) \to 0$ and $g(r,\theta) \to 0$ at least as fast as r.

Because $v_c(r,\theta)$ is bounded, proving that $\dot{\hat{\boldsymbol{r}}}|_{\dot{\boldsymbol{r}}=\boldsymbol{h}}$ is bounded will prove that Eq. (53) is the integral of a piecewise continuous bounded function, and therefore $\boldsymbol{c}(\boldsymbol{r}, \hat{\boldsymbol{o}}) = v_c(r,\theta)\hat{\boldsymbol{r}}$ is Lipschitz continuous in time. Taking the derivative of $\hat{\boldsymbol{r}}$ yields

$$\begin{aligned}\dot{\hat{\boldsymbol{r}}}|_{\dot{\boldsymbol{r}}=\boldsymbol{h}} &= \frac{d\hat{\boldsymbol{r}}}{d\boldsymbol{r}}\dot{\boldsymbol{r}}|_{\dot{\boldsymbol{r}}=\boldsymbol{h}} = \left(\frac{\boldsymbol{I} - \hat{\boldsymbol{r}}\hat{\boldsymbol{r}}^T}{r}\right)(v_c(r,\theta)\hat{\boldsymbol{r}} + s_a(r,\theta)\hat{\boldsymbol{a}} \\ &\quad + g(r,\theta)\boldsymbol{\omega}_{OI}^{\times}\hat{\boldsymbol{r}}) = \frac{s_a(r,\theta)\hat{\boldsymbol{a}} + g(r,\theta)\boldsymbol{\omega}_{OI}^{\times}\hat{\boldsymbol{r}}}{r}\end{aligned} \tag{57}$$

which is already bounded by the conditions that $\boldsymbol{\omega}_{OI}$, $s_a(r,\theta)/r$, and $g(r,\theta)/r$ are bounded.

Next, let us examine the conditions required for $\boldsymbol{a}(\boldsymbol{r}, \hat{\boldsymbol{o}}) = s_a(r,\theta)\hat{\boldsymbol{a}}$ to be Lipschitz time continuous. Analogous to the previous developments, we begin with

$$\Delta\boldsymbol{a} = \Delta(s_a(r,\theta)\hat{\boldsymbol{a}}) = \sum\int(\dot{s}_a(r,\theta)\hat{\boldsymbol{a}} + s_a(r,\theta)\dot{\hat{\boldsymbol{a}}})\,\mathrm{d}t \tag{58}$$

Noting that $\dot{r}|_{\dot{\boldsymbol{r}}=\boldsymbol{h}}$ and $\dot{\theta}|_{\dot{\boldsymbol{r}}=\boldsymbol{h}}$ are already bounded and that $s_a(r,\theta)$ is assumed to be Lipschitz in r and θ, it immediately follows that $\dot{s}_a(r,\theta)|_{\dot{\boldsymbol{r}}=\boldsymbol{h}}$ is bounded (and indeed, so is $\dot{g}(r,\theta)|_{\dot{\boldsymbol{r}}=\boldsymbol{h}}$). Therefore it is sufficient to show that the product $s_a(r,\theta)\dot{\hat{\boldsymbol{a}}}|_{\dot{\boldsymbol{r}}=\boldsymbol{h}}$ is bounded. To show this, let us derive the time derivative of $\hat{\boldsymbol{a}}$:

$$\dot{\hat{\boldsymbol{a}}} = \frac{\partial\hat{\boldsymbol{a}}}{\partial\hat{\boldsymbol{r}}}\dot{\hat{\boldsymbol{r}}} + \frac{\partial\hat{\boldsymbol{a}}}{\partial\hat{\boldsymbol{o}}}\dot{\hat{\boldsymbol{o}}} \tag{59}$$

where

$$\begin{aligned}\frac{\partial\hat{\boldsymbol{a}}}{\partial\hat{\boldsymbol{r}}} &= \frac{d\hat{\boldsymbol{a}}}{d(\hat{\boldsymbol{o}}\hat{\boldsymbol{r}}^T\hat{\boldsymbol{r}} - \hat{\boldsymbol{r}}\hat{\boldsymbol{r}}^T\hat{\boldsymbol{o}})}\frac{\partial(\hat{\boldsymbol{o}}\hat{\boldsymbol{r}}^T\hat{\boldsymbol{r}} - \hat{\boldsymbol{r}}\hat{\boldsymbol{r}}^T\hat{\boldsymbol{o}})}{\partial\hat{\boldsymbol{r}}} \\ &= \left(\frac{\boldsymbol{I} - \hat{\boldsymbol{a}}\hat{\boldsymbol{a}}^T}{\sin\theta}\right)(2\hat{\boldsymbol{o}}\hat{\boldsymbol{r}}^T - \hat{\boldsymbol{r}}\hat{\boldsymbol{o}}^T - \hat{\boldsymbol{r}}^T\hat{\boldsymbol{o}}\boldsymbol{I})\end{aligned} \tag{60}$$

and similarly

$$\frac{\partial\hat{\boldsymbol{a}}}{\partial\hat{\boldsymbol{o}}} = \left(\frac{\boldsymbol{I} - \hat{\boldsymbol{a}}\hat{\boldsymbol{a}}^T}{\sin\theta}\right)(\boldsymbol{I} - \hat{\boldsymbol{r}}\hat{\boldsymbol{r}}^T) \tag{61}$$

Substituting Eq. (57) into Eq. (59) and simplifying yields

$$\dot{\hat{\boldsymbol{a}}}|_{\dot{\boldsymbol{r}}=\boldsymbol{h}} = \frac{-s_a(r,\theta) - g(r,\theta)\boldsymbol{\omega}_{OI}^T\hat{\boldsymbol{e}}}{r}\hat{\boldsymbol{r}} + \frac{g(r,\theta)\cos\theta\boldsymbol{\omega}_{OI}^T\hat{\boldsymbol{a}}}{r\sin\theta}\hat{\boldsymbol{e}} + \frac{\boldsymbol{\omega}_{OI}^T(\hat{\boldsymbol{r}}\sin\theta - \hat{\boldsymbol{a}}\cos\theta)}{\sin\theta}\hat{\boldsymbol{e}} \tag{62}$$

Therefore, the product $s_a(r,\theta)\dot{\hat{\boldsymbol{a}}}|_{\dot{\boldsymbol{r}}=\boldsymbol{h}}$ is bounded only if $s_a(r,\theta)/\sin\theta$ is bounded (which also implies that $s_a(r,\theta)$ is bounded). Therefore, if $\theta \to 0$ or $\theta \to \pi$, then it is required that $s_a(r,\theta) \to 0$ at least as quickly as $\sin\theta \to 0$.

Lastly, let us solve for constraints that ensure that $\boldsymbol{g}(\boldsymbol{r},\hat{\boldsymbol{o}},\boldsymbol{\omega}_{OI})$ is Lipschitz time continuous. Again, assuming a bounded piecewise continuous derivative

$$\Delta\boldsymbol{g} = \Delta(g(r,\theta)\boldsymbol{\omega}_{OI}^{\times}\hat{\boldsymbol{r}}) = \sum\int(\dot{g}(r,\theta)\boldsymbol{\omega}_{OI}^{\times}\hat{\boldsymbol{r}} + g(r,\theta)\dot{\boldsymbol{\omega}}_{OI}^{\times}\hat{\boldsymbol{r}} + g(r,\theta)\boldsymbol{\omega}_{OI}^{\times}\dot{\hat{\boldsymbol{r}}})\,\mathrm{d}t \tag{63}$$

where $\dot{g}(r,\theta)|_{\dot{\boldsymbol{r}}=\boldsymbol{h}}$ is already bounded, $\dot{\boldsymbol{\omega}}_{OI}$ must be bounded to be trackable, and $\dot{\hat{\boldsymbol{r}}}|_{\dot{\boldsymbol{r}}=\boldsymbol{h}}$ is already bounded. Therefore, $\boldsymbol{g}$ is Lipschitz continuous if $g(r,\theta)$ is bounded. Because $\dot{\boldsymbol{d}}$ is the motion of a real object, it is also Lipschitz continuous. Furthermore, it is assumed for the use of CLVFs that $\ddot{\boldsymbol{d}}$ is relatively small compared to the acceleration capabilities of the controlled vehicle. Therefore, to guarantee an upper acceleration bound $u_{\max}$ on perfect tracking of the simplified CLVF given by Eq. (49), it is sufficient that the following conditions are met:

E1) $v_c(r,\theta)$ is bounded and is globally Lipschitz continuous in r and θ.

E2) $g(r,\theta)$ is bounded and is globally Lipschitz continuous in r and θ. Furthermore, $g(r,\theta)/r$ is bounded.

E3) $s_a(r,\theta)$ is bounded and is globally Lipschitz continuous in r and θ. Furthermore, $s_a(r,\theta)/r$ and $s_a(r,\theta)/\sin\theta$ are bounded.

E. Feed-Forward Acceleration Equations

Here, let us find feed-forward acceleration equations for the CLVF. The purpose of these equations is twofold. Firstly, these equations can be used to bound the acceleration limit $u_{\max}$. Secondly, these equations can be used as a feed-forward acceleration to help track the CLVF.

Utilizing the chain rule on Eq. (49), we arrive at the following general feed-forward acceleration expression on the intervals where $\boldsymbol{h}$ is differentiable:

$$\dot{\boldsymbol{h}}(\boldsymbol{r},\hat{\boldsymbol{o}},\boldsymbol{\omega}_{OI},\dot{\boldsymbol{d}}) = \dot{v}_c\hat{\boldsymbol{r}} + v_c\dot{\hat{\boldsymbol{r}}} + \dot{s}_a\hat{\boldsymbol{a}} + s_a\dot{\hat{\boldsymbol{a}}} + \dot{g}\boldsymbol{\omega}_{OI}^{\times}\hat{\boldsymbol{r}} + g\dot{\boldsymbol{\omega}}_{OI}^{\times}\hat{\boldsymbol{r}} + g\boldsymbol{\omega}_{OI}^{\times}\dot{\hat{\boldsymbol{r}}} + \ddot{\boldsymbol{d}} \tag{64}$$

where arguments have been dropped for notational simplicity. Assuming that the CLVF is tracked by the controlled spacecraft,

$$\dot{\boldsymbol{h}}(\boldsymbol{r},\hat{\boldsymbol{o}},\boldsymbol{\omega}_{OI},\dot{\boldsymbol{d}})|_{\dot{\boldsymbol{r}}=\boldsymbol{h}} = (\dot{v}_c|_{\dot{\boldsymbol{r}}=\boldsymbol{h}})\hat{\boldsymbol{r}} + v_c(\dot{\hat{\boldsymbol{r}}}|_{\dot{\boldsymbol{r}}=\boldsymbol{h}}) + (\dot{s}_a|_{\dot{\boldsymbol{r}}=\boldsymbol{h}})\hat{\boldsymbol{a}} + s_a(\dot{\hat{\boldsymbol{a}}}|_{\dot{\boldsymbol{r}}=\boldsymbol{h}}) + (\dot{g}|_{\dot{\boldsymbol{r}}=\boldsymbol{h}})\boldsymbol{\omega}_{OI}^{\times}\hat{\boldsymbol{r}} + g\dot{\boldsymbol{\omega}}_{OI}^{\times}\hat{\boldsymbol{r}} + g\boldsymbol{\omega}_{OI}^{\times}(\dot{\hat{\boldsymbol{r}}}|_{\dot{\boldsymbol{r}}=\boldsymbol{h}}) + \ddot{\boldsymbol{d}} \tag{65}$$

After substituting Eq. (57) and Eq. (62) into Eq. (65) and simplifying, Eq. (65) can be put into the following form:

$$\dot{\boldsymbol{h}}(\boldsymbol{r},\hat{\boldsymbol{o}},\boldsymbol{\omega}_{OI},\dot{\boldsymbol{d}})|_{\dot{\boldsymbol{r}}=\boldsymbol{h}} = \phi_1(r,\theta)\hat{\boldsymbol{r}} + \phi_2(r,\theta)\hat{\boldsymbol{a}} + \boldsymbol{\omega}_{OI}^{\times}\Omega_1(\boldsymbol{r},\hat{\boldsymbol{o}}) + \Omega_2(\boldsymbol{r},\hat{\boldsymbol{o}},\boldsymbol{\omega}_{OI}) + \frac{g^2(r,\theta)}{r}\boldsymbol{\omega}_{OI}^{\times}\boldsymbol{\omega}_{OI}^{\times}\hat{\boldsymbol{r}} + g(r,\theta)\dot{\omega}_{OI}^{\times}\hat{\boldsymbol{r}} + \ddot{\boldsymbol{d}} \tag{66}$$

where

$$\phi_1(r,\theta) = \dot{v}_c(r,\theta)|_{\dot{\boldsymbol{r}}=\boldsymbol{h}} - \frac{s_a^2(r,\theta)}{r} \tag{67}$$

$$\phi_2(r,\theta) = \dot{s}_a(r,\theta)|_{\dot{\boldsymbol{r}}=\boldsymbol{h}} + \frac{s_a(r,\theta)v_c(r,\theta)}{r} \tag{68}$$

$$\boldsymbol{\Omega}_1(\boldsymbol{r},\hat{\boldsymbol{o}}) = \left(\dot{g}(r,\theta)|_{\dot{\boldsymbol{r}}=\boldsymbol{h}} + \frac{g(r,\theta)}{r}v_c(r,\theta)\right)\hat{\boldsymbol{r}} + \left(s_a(r,\theta) + \frac{g(r,\theta)}{r}s_a(r,\theta)\right)\hat{\boldsymbol{a}} \tag{69}$$

$$\boldsymbol{\Omega}_2(\boldsymbol{r},\hat{\boldsymbol{o}},\boldsymbol{\omega}_{OI}) = s_a(r,\theta)\left(1 - \frac{g(r,\theta)}{r}\right)\left(\hat{\boldsymbol{r}}\boldsymbol{\omega}_{OI}^T\hat{\boldsymbol{e}} - \frac{\cos\theta}{\sin\theta}\hat{\boldsymbol{e}}\boldsymbol{\omega}_{OI}^T\hat{\boldsymbol{a}}\right) \tag{70}$$

Note that if $g(r,\theta) = r$ (which of course does not meet the acceleration constraint E2), then Eqs. (69) and (70) reduce to

$$\boldsymbol{\Omega}_1(\boldsymbol{r},\hat{\boldsymbol{o}}) = 2v_c(r,\theta)\hat{\boldsymbol{r}} + 2s_a(r,\theta)\hat{\boldsymbol{a}} \tag{71}$$

$$\boldsymbol{\Omega}_2(\boldsymbol{r},\hat{\boldsymbol{o}},\boldsymbol{\omega}_{OI}) = \boldsymbol{0} \tag{72}$$

By observation of the other terms, it is clear that a selection of $g(r,\theta) = r$ reduces the equations to the familiar form of feed-forward accelerations used for tracking within a rotating reference frame. Indeed, tracking the rotating reference frame upon arrival to $\mathbb{A}_c$ is the purpose of D2. Likewise, although not mandated, a well-designed set of functions $g(r,\theta)$ and $s_a(r,\theta)$ will approach 0 as $r \to \infty$. Therefore, very far from the target, Eq. (66) simply becomes

$$\dot{\boldsymbol{h}}(\boldsymbol{r},\hat{\boldsymbol{o}},\boldsymbol{\omega}_{OI},\dot{\boldsymbol{d}})|_{\dot{\boldsymbol{r}}=\boldsymbol{h}} = (\dot{v}_c(r,\theta)|_{\dot{\boldsymbol{r}}=\boldsymbol{h}})\hat{\boldsymbol{r}} + \ddot{\boldsymbol{d}} \tag{73}$$

which is a contraction in the inertial frame. Therefore, for values of r between ∞ and α, Eq. (66) is an acceleration-bounded feed-forward equation designed to transition from an inertial contraction into a body-fixed trajectory.

F. Tracking the CLVF with Saturation

Provided that no saturation occurs, Eq. (7) proposed by [10] is still a globally asymptotically stable controller for tracking CLVFs by the same proof (Theorem 2 in this paper). However, although Eqs. (66–70) may be used to ensure that $\|\dot{\boldsymbol{h}}\|_{\dot{\boldsymbol{r}}=\boldsymbol{h}}$ (acceleration under perfect tracking) is bounded, there is no guarantee that $\|\dot{\boldsymbol{h}}\|$ (time derivative of the CLVF during general motion) is bounded. Furthermore, because this controller uses a constant gain β, for sufficiently large tracking error the acceleration commands will saturate. Therefore, it is worthwhile to study the effects of saturation on Theorem 2. First, let us assume that the actual acceleration controller is given by

$$\ddot{\boldsymbol{r}} = \begin{cases} \boldsymbol{u}, & \|\boldsymbol{u}\| \le u_{\max}, \\ \left(\dfrac{u_{\max}}{\|\boldsymbol{u}\|}\right)\boldsymbol{u}, & \text{otherwise} \end{cases} \tag{74}$$

where $\boldsymbol{u}$ is still defined as

$$\boldsymbol{u} = -\beta(\dot{\boldsymbol{r}} - \boldsymbol{h}) + \dot{\boldsymbol{h}} \tag{75}$$

Let us return to the control Lyapunov function W given by Eq. (8) with the time derivative given by Eq. (9). Substituting Eq. (74) into Eq. (9) assuming saturation gives

$$\dot{W} = -\beta\left(\frac{u_{\max}}{\|\boldsymbol{u}\|}\right)(\dot{\boldsymbol{r}} - \boldsymbol{h})^T(\dot{\boldsymbol{r}} - \boldsymbol{h}) - (\dot{\boldsymbol{r}} - \boldsymbol{h})^T\left(1 - \frac{u_{\max}}{\|\boldsymbol{u}\|}\right)\dot{\boldsymbol{h}} \tag{76}$$

which has the potential to become positive if

$$\left(1-\frac{u_{\max}}{\|\boldsymbol{u}\|}\right)\|\dot{\boldsymbol{h}}\| > \beta\left(\frac{u_{\max}}{\|\boldsymbol{u}\|}\right)\|\dot{\boldsymbol{r}}-\boldsymbol{h}\| \tag{77}$$

At this point, recall that one of the assumptions motivating CLVFs is that the controlled vehicle is initialized reasonably far away from the target, and therefore tracking the target attitude is unreasonable. If $g(r,\theta)$ and $s_a(r,\theta)$ are well-designed, it can be assumed that $g(r,\theta)\to 0$ and $s_a(r,\theta)\to 0$ as $r\to\infty$. Therefore, for a sufficiently large distance

$$\boldsymbol{h}(\boldsymbol{r},\boldsymbol{o},\boldsymbol{\omega}_{OI},\dot{\boldsymbol{d}}) \approx v_c(r,\theta)\hat{\boldsymbol{r}}+\dot{\boldsymbol{d}} \tag{78}$$

In the spacecraft case, so long as the target and chaser begin with a separation distance that is far less than the orbital radius, a non-rotating reference frame fixed to the target spacecraft's center of mass can be approximated as inertial from the chasers perspective, and $\dot{\boldsymbol{d}}=\boldsymbol{0}$ in this reference frame. Furthermore, it is known from E1 that $v_c(r,\theta)$ is bounded. It is reasonable to assume that $\|v_c(r,\theta)\|$ is maximized for large distances, and therefore $\dot{v}_c(r,\theta)\approx 0$. Therefore, knowledge of CLVF applications leads to the reasonable assumption that when the controller is initialized, the controlled vehicle will be distant from the target, and

$$\dot{\boldsymbol{h}} \approx \boldsymbol{0} \tag{79}$$

regardless of velocity errors that may be present at initialization. Therefore, under standard initialization conditions, saturated thrusters result in the following approximate time-derivative of the control Lyapunov function:

$$\dot{W} \approx -u_{\max}(\dot{\boldsymbol{r}}-\boldsymbol{h})^T(\dot{\boldsymbol{r}}-\boldsymbol{h}) \tag{80}$$

For reasonable values of $u_{\max}$, it may be assumed that the error dynamics decay below saturation levels well before the chaser and target are close enough together that Eq. (79) becomes a poor assumption.

V. Design Procedure and Simulations

In this section, a full CLVF design is performed for a spacecraft performing a close-proximity inspection of a spinning target. The design is repeated for various values of $u_{\max}$, and results are presented for three different sets of initial conditions. The design procedure employed is as follows:

1) Design the functions $v_c(r,\theta)$, $s_a(r,\theta)$, and $g(r,\theta)$ according to the desired behavior while meeting stability constraints D1–D3 and acceleration constraints E1–E3. Leave some parameters in these functions unknown.

2) Using Eqs. (66–70), solve for an acceleration bound as a function of the unknown parameters from step 1.

3) Using the acceleration bound function from step 2, perform a parameter optimization such that the bounded acceleration is less than or equal to $u_{\max}$.

Note that, for simplicity, the parameter optimization shown in this paper is a simple line search, where only total acceleration is constrained. This could, however, be easily expanded. For example, velocity could be constrained by placing upper bound constraints on the parameters k_c and k_a. Furthermore, other metrics such as fuel usage, maneuver time, or maximum jerk could all be considered by estimating these quantities as functions of the CLVF parameters and including penalties in an optimization cost function.

A. Scenario Description

For simplicity of presentation, let us assume in the following that the chaser spacecraft approaches the target spacecraft in the plane defined by the target spin vector (note that the full three-dimensional case follows completely analogously). The goal of the chaser is to contract to a radius of $\alpha = 10$ m, and repetitively inspect each of the four sides of the target while it spins. Example time-lapse images of this trajectory are presented in the target body-fixed frame in Fig. 3.

The chaser spacecraft is set to observe each side of the target for 30 s. Between these 30 s pauses, the desired angle between the chaser and the target increases by $\pi/2$ rad over a 30 s period. That is, the rotation of the desired trajectory in the body-fixed frame is

$$\omega_{OB}(t) = \begin{cases} 0.0 \text{ rad/s}, & \text{during inspections} \\ (0.01047t_d - 0.00034907t_d^2) \text{ rad/s}, & \text{when changing inspection angle} \end{cases} \tag{81}$$

where t_d is the time that has elapsed since departing the previous inspection angle. The spin rate of the target spacecraft is constant, defined as

$$\omega_{BI} = 0.1 \text{ rad/s} \tag{82}$$

B. Design of the CLVF

Let us now perform the design procedure according to the steps outlined at the start of this section.

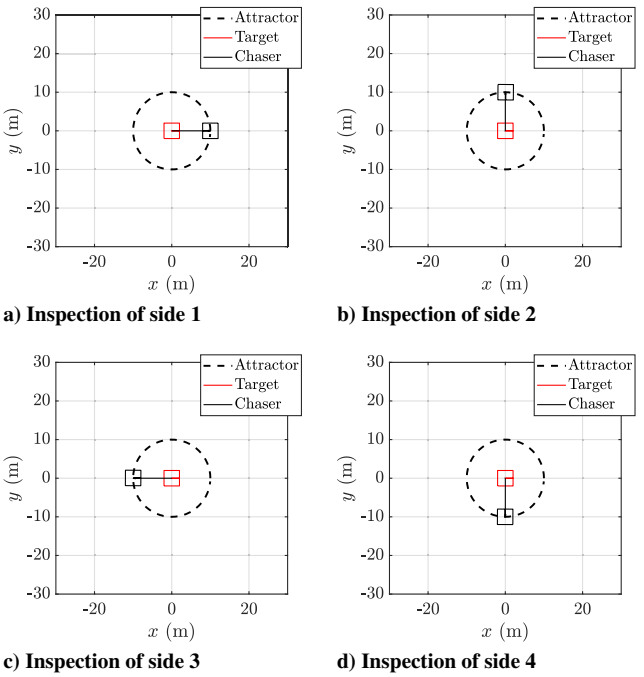

a) Inspection of side 1 b) Inspection of side 2

c) Inspection of side 3 d) Inspection of side 4

Fig. 3 Desired inspection trajectory.

1. Design of Speed and Distance Functions

The following function is selected for $g(r,\theta)$:

$$g(r) = \begin{cases} r, & r < \alpha \\ \dfrac{\alpha^2}{r}, & \text{otherwise} \end{cases} \tag{83}$$

which clearly meets the requirements of D2 and E2. This function also has the property that $g(\infty) = 0$, which is beneficial for fuel expenditure. Furthermore, this selection will simplify finding an acceleration bound, as when the chaser is tracking perfectly and approaching from outside of the attractor, it can be seen that

$$\dot{g}(r)|_{\dot{\boldsymbol{r}}=\boldsymbol{h}} = -\frac{g(r)}{r} v_c(r,\theta) \tag{84}$$

which cancels a term in Eq. (69). Next, following the constraints of D3 and E3, let us select $s_a(r,\theta)$ as

$$s_a(r,\theta) = \begin{cases} k_a \dfrac{r}{\alpha}\sin\theta, & r < \alpha \\ k_a \dfrac{\alpha}{r}\sin\theta, & \text{otherwise} \end{cases} \tag{85}$$

where, following the design procedure step 1, k_a is an unselected strictly positive parameter. Likewise, let us select the velocity function that meets D1 and E1 as

$$v_c(r) = \begin{cases} k_c \dfrac{\alpha - r}{b}, & \|\alpha - r\| < b \\ k_c \text{sgn}(\alpha - r), & \text{otherwise} \end{cases} \tag{86}$$

where k_c and b are unselected strictly positive parameters. Therefore, by the constraints D1–D3 the CLVF will inherit asymptotic stability, and by E1–E3 there will be an upper bound on the required acceleration for perfect tracking. By finding a suitable k_a, k_c, and b, the upper bound on tracking acceleration for this field can adjusted to meet $u_{\max}$.

2. Finding a Function for the Upper Bound in Terms of k_a, k_c, and b

In general, the acceleration bound when approaching from the inside of the attractor $\mathbb{A}$ will *not* be equal to the acceleration bound when approaching from the outside. Because it is assumed that the chaser spacecraft approaches from the outside, this is the bound we will search for.

To begin, let us make some simplifications to Eq. (66). First, the selection of $g(r)$ will cancel a term in Eq. (69) as previously discussed. Secondly, because both spacecraft experience roughly equal acceleration due to gravity, the acceleration of the target is approximated by $\ddot{\boldsymbol{d}} \approx \boldsymbol{0}$. Lastly, because the scenario is planar, $\boldsymbol{\omega}_{OI}$ will be entirely along the $\hat{\boldsymbol{e}}$ direction. Making these simplifications and rearranging, Eq. (66) reduces to

$$\dot{\boldsymbol{h}}(\boldsymbol{r},\hat{\boldsymbol{o}},\boldsymbol{\omega}_{OI},\dot{\boldsymbol{d}})|_{\dot{\boldsymbol{r}}=\boldsymbol{h}} = \left(\dot{v}_c|_{\dot{\boldsymbol{r}}=\boldsymbol{h}} - \frac{(s_a + g\omega_{OI})^2}{r}\right)\hat{\boldsymbol{r}} + (\dot{s}_a|_{\dot{\boldsymbol{r}}=\boldsymbol{h}} + \frac{s_a v_c}{r} + g\dot{\omega}_{OI})\hat{\boldsymbol{a}} \tag{87}$$

where arguments are dropped for simplicity. After some straightforward time derivatives of each function (assuming perfect tracking) and substitution into Eq. (87), the following somewhat conservative bound is attained:

$$\|\dot{\boldsymbol{h}}\|_{\dot{\boldsymbol{r}}=\boldsymbol{h}} < \left(\left[\frac{k_c^2}{b} + \frac{(k_a + \alpha\omega_{\max})^2}{\alpha}\right]^2 + \left[\frac{k_a^2}{2\alpha} + k_a\omega_{\max} + \alpha\dot{\omega}_{\max}\right]^2\right)^{1/2} \tag{88}$$

where $\omega_{\max}$ and $\dot{\omega}_{\max}$ are the maximum norms of the vectors $\boldsymbol{\omega}_{OI}$ and $\dot{\boldsymbol{\omega}}_{OI}$, respectively. That is, for the general tumbling case

$$\omega_{\max} = \|\boldsymbol{\omega}_{BI}^B + \boldsymbol{C}_{BO}\boldsymbol{\omega}_{OB}^O\|_{\max} \tag{89}$$

$$\dot{\omega}_{\max} = \|\dot{\boldsymbol{\omega}}_{BI}^B + \boldsymbol{C}_{BO}\dot{\boldsymbol{\omega}}_{OB}^O\|_{\max} \tag{90}$$

Alternatively, given that the chaser spacecraft has an acceleration limit $u_{\max}$, we want to find a set of parameters (k_a, k_c, b) such that the following inequality is satisfied:

$$u_{\max} \geq \left(\left[\frac{k_c^2}{b} + \frac{(k_a + \alpha\omega_{\max})^2}{\alpha}\right]^2 + \left[\frac{k_a^2}{2\alpha} + k_a\omega_{\max} + \alpha\dot{\omega}_{\max}\right]^2\right)^{1/2} \tag{91}$$

It is useful to note that over the domain where k_a, k_c, and b are all strictly greater than 0, Eq. (91) forms a convex set, and therefore any of the widely known convex search algorithms can be used in the selection of parameters.

3. Selection of Parameters According to the Acceleration Limit $u_{\max}$

For simplicity, a line search is used as the parameter selection algorithm; details beyond what is presented here for this algorithm, including alternative versions of the line search, can be found in [18]. Note that a more well-designed convex optimization method would result in better parameter selections, which can generally be used to reduce fuel consumption, reduce convergence time, and add jerk penalties or any other cost penalties. These more advanced optimizations, however, are beyond the scope of this work. Initial search values for the parameters are taken as $k_a = 0.5$ m/s, $k_c = 0.0$ m/s, and $b = 5$ m. The line-search direction was arbitrarily selected as

$$[\,\Delta k_a \quad \Delta k_c \quad \Delta b\,] = [\,0.1 \quad 0.1 \quad -0.5\,]\gamma \tag{92}$$

where γ is some varying step size. This line is searched until a combination (k_a, k_c, b) is found such that Eq. (91) holds with equality. Of course, if the bound described by Eq. (91) is loose, then the actual acceleration required may be far less than $u_{\max}$. Therefore, to take full advantage of the available thrust, the designer should use all available information to find a bound that is as tight as possible. Of course, some looseness in the bound does provide margin before the thrusters saturate, which may be advantageous in many practical scenarios. By considering multiple values for $u_{\max}$, Table 1 summarizes the resulting parameters from the line search.

C. Results

For each acceleration constraint and corresponding parameter selections from Table 1, three different initial conditions are tested (listed in Table 2). These conditions vary the chaser

Table 1 Parameter selection for spacecraft with varying acceleration constraints

$u_{\max}$, m/s^2	k_a, m/s	k_c, m/s	b, m
5.0	1.454	0.9537	0.2315
3.0	1.414	0.9139	0.4303
1.0	1.0495	0.5495	2.253
0.7	0.7226	0.2336	3.832

Table 2 Initial conditions

Case	Initial position, m	Initial velocity, m/s^2	Initial target angle, rad	Initial trajectory angle, rad
1	$[-20 \quad 30]^T$	$[0 \quad 0]^T$	0	π
2	$[20 \quad -15]^T$	$[-0.8 \quad -0.5]^T$	$-\pi/4$	0
3	$[30 \quad 15]^T$	$[0 \quad 0]^T$	0	0

vehicles initial position and velocity, and also vary the initial angle of the target in the world frame, and the initial angle of $\hat{\boldsymbol{o}}^B$ relative to the x vector of the target body-fixed frame. In every case, the controller gain value was selected as $\beta = 0.05\ \mathrm{s}^{-1}$, corresponding to a velocity error decay time constant of 20 s. This small value is selected because after the chaser is tracking the CLVF, most of the control input is handled by the feed-forward acceleration equations. In a scenario with perturbations and imperfect measurements, a larger bandwidth for β may be desired dependent on the tracking-accuracy needs, just as is done for standard controller design.

Figures 4–7 show the resulting acceleration, convergence in r, and convergence in θ for each acceleration constraint and set of initial conditions. For case 1, time-lapse images of the chaser spacecraft with an acceleration constraint of $u_{\max} = 5\ \mathrm{m/s^2}$ and $u_{\max} = 0.7\ \mathrm{m/s^2}$ are provided, respectively, in Figs. 8 and 9.

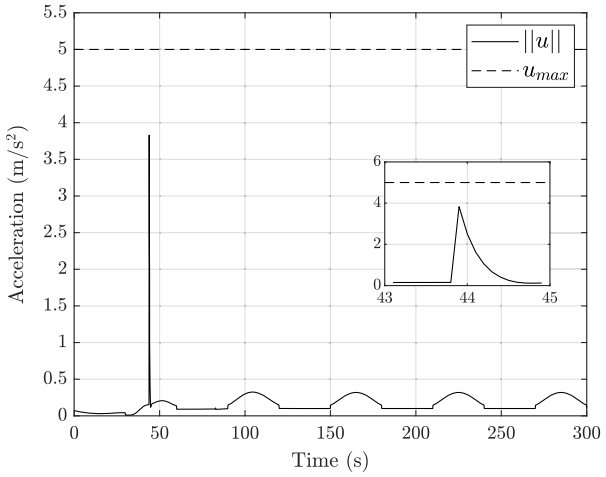

a) Acceleration norm over time - Case 1

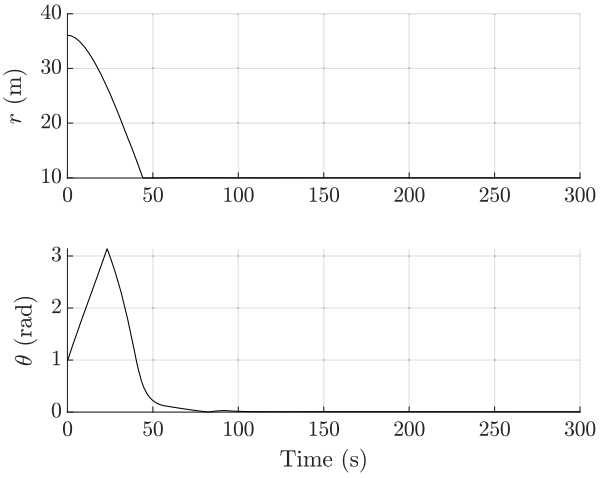

b) Convergence of r and θ over time - Case 1

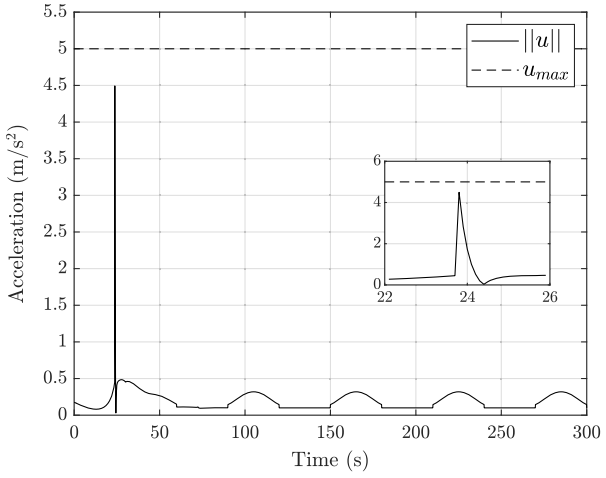

c) Acceleration norm over time - Case 2

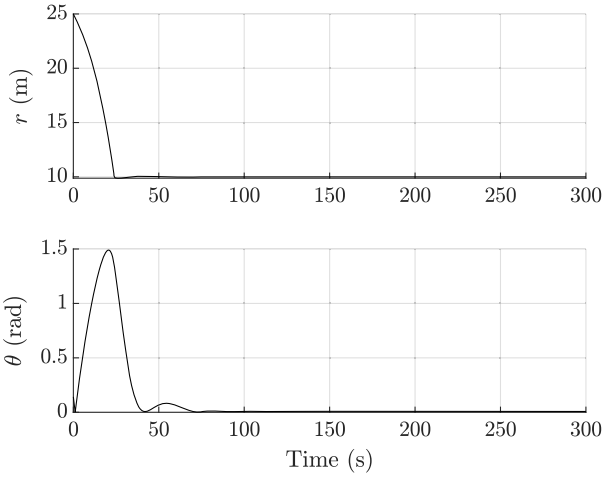

d) Convergence of r and θ over time - Case 2

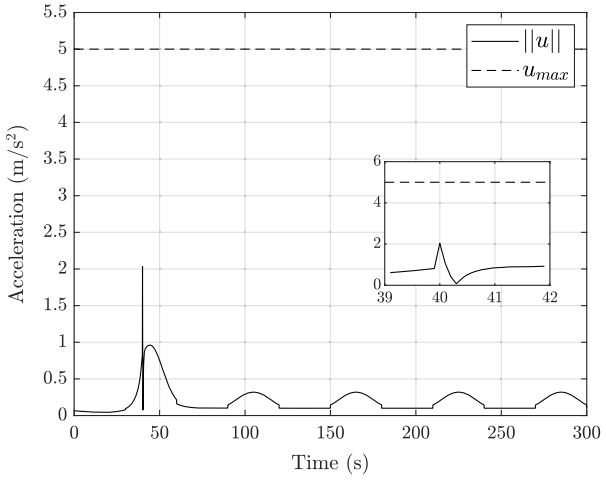

e) Acceleration norm over time - Case 3

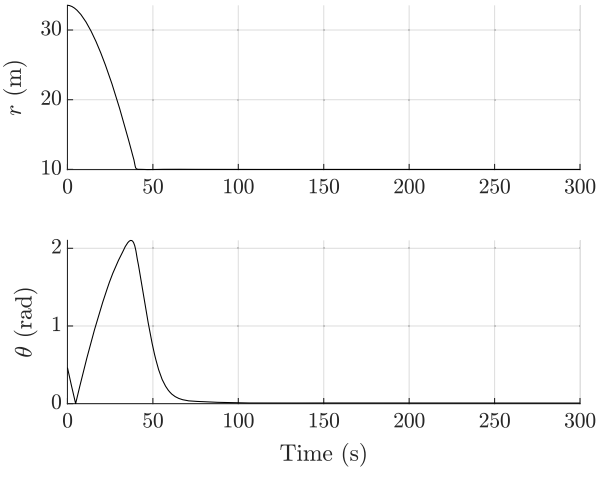

f) Convergence of r and θ over time - Case 3

Fig. 4 Maximum acceleration constraint: $u_{\max} = 5.0\ \mathrm{m/s^2}$.

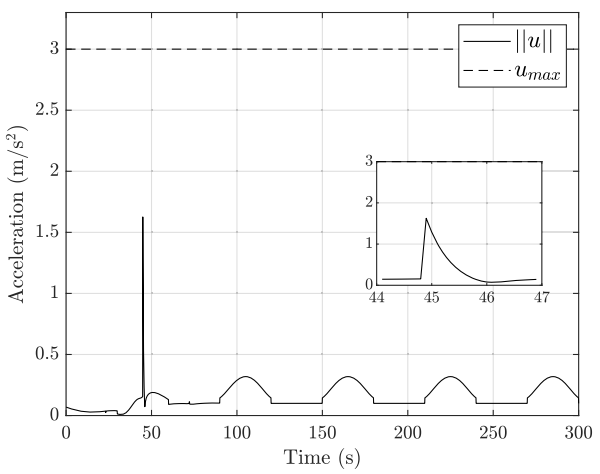

a) Acceleration norm over time - Case 1

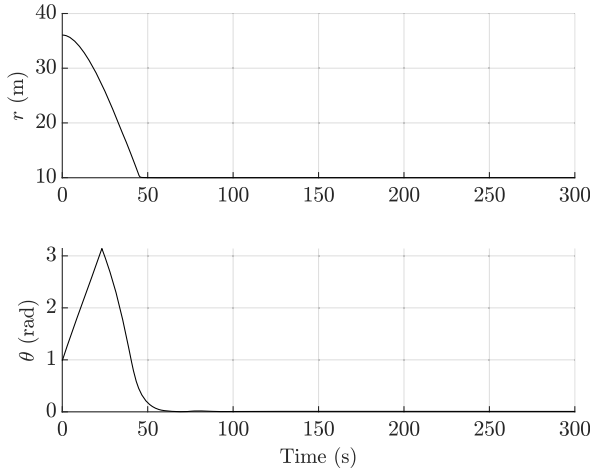

b) Convergence of r and θ over time - Case 1

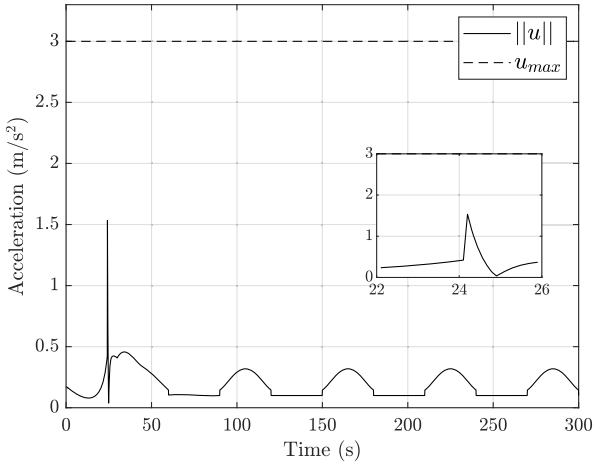

c) Acceleration norm over time - Case 2

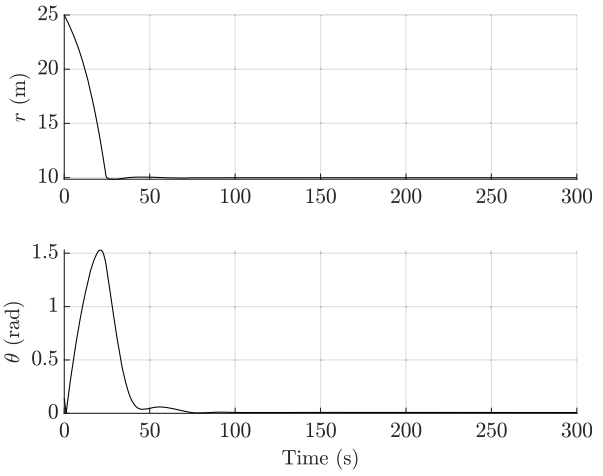

d) Convergence of r and θ over time - Case 2

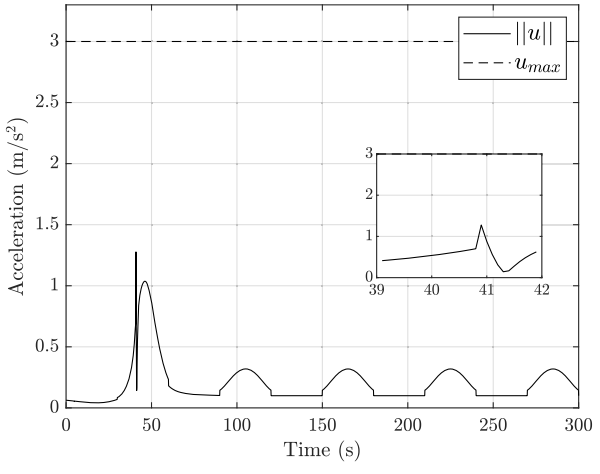

e) Acceleration norm over time - Case 3

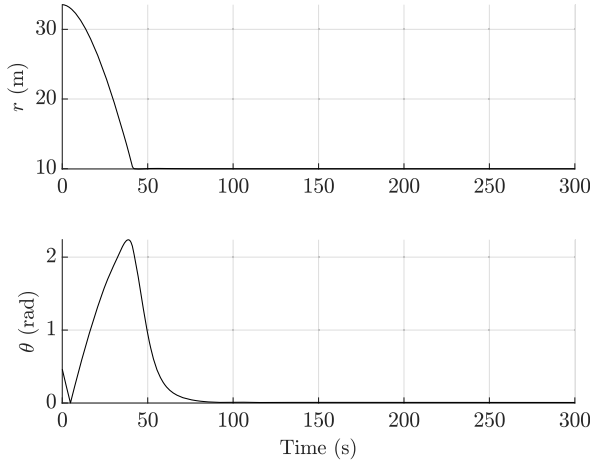

f) Convergence of r and θ over time - Case 3

Fig. 5 Maximum acceleration constraint: $u_{\max} = 3.0$ m/s^2.

As intended, for each case the actual acceleration stays within the vehicle acceleration constraint $u_{\max}$. Furthermore, the expected behavior of convergence in r followed by convergence in θ occurred for every value of $u_{\max}$ and under every tested set of initial conditions. However, for higher values of $u_{\max}$ the parameter search resulted in CLVFs where there was potential for more agile maneuvering, resulting in faster convergence. Intuitively, this means that vehicles with higher acceleration capabilities have a broader parameter selection to choose from, giving the opportunity for a design tradeoff between maneuver duration and fuel expenditure. Indeed, the time-lapse images in Figs. 8 and 9 show that the $u_{\max} = 5$ m/s^2 vehicle selects a path that converges much faster than the $u_{\max} = 0.7$ m/s^2 vehicle under identical initial conditions. Of course, finding a tighter bound than Eq. (91) would result in a larger set of permissible parameters for any given $u_{\max}$, resulting in more design options and potentially fuller use of the vehicles' acceleration capabilities.

By comparing the acceleration norm results under different initial conditions for the same set of CLVF parameters (e.g., Figs. 4c and 4e),

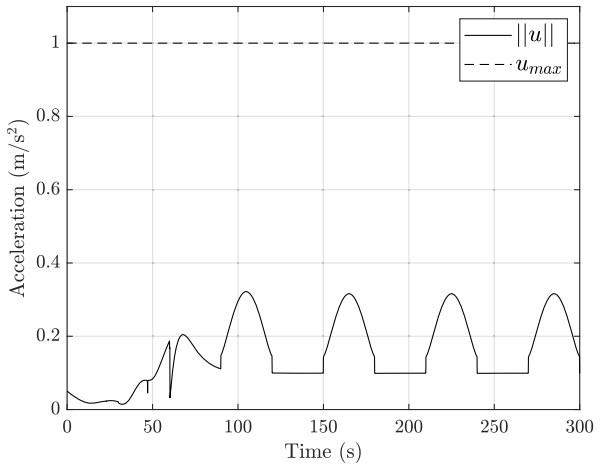

a) Acceleration norm over time - Case 1

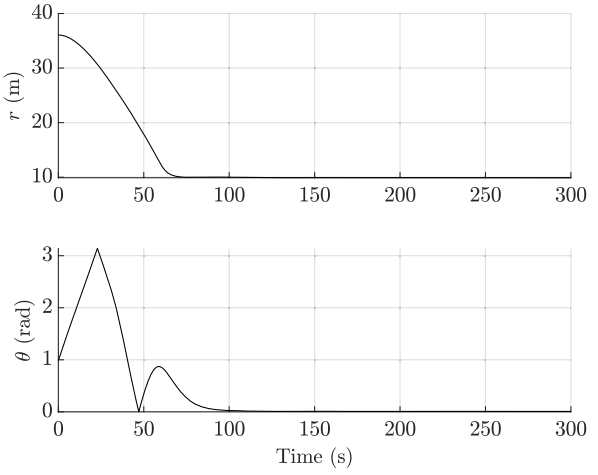

b) Convergence of r and θ over time - Case 1

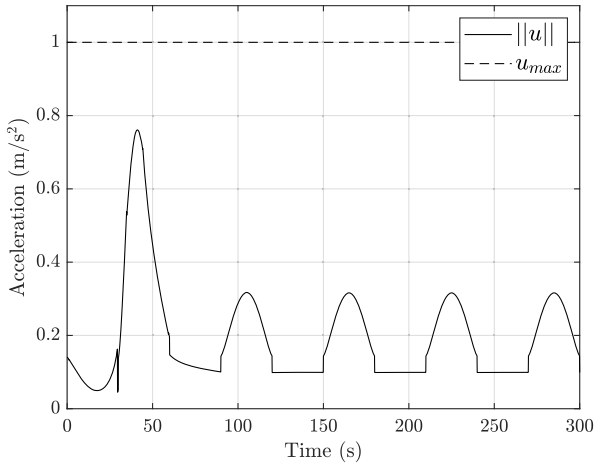

c) Acceleration norm over time - Case 2

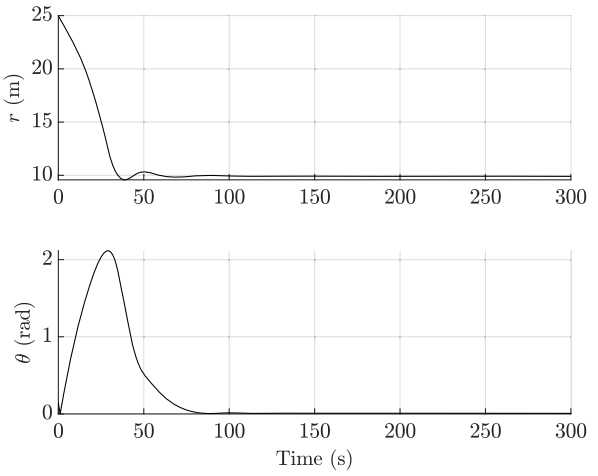

d) Convergence of r and θ over time - Case 2

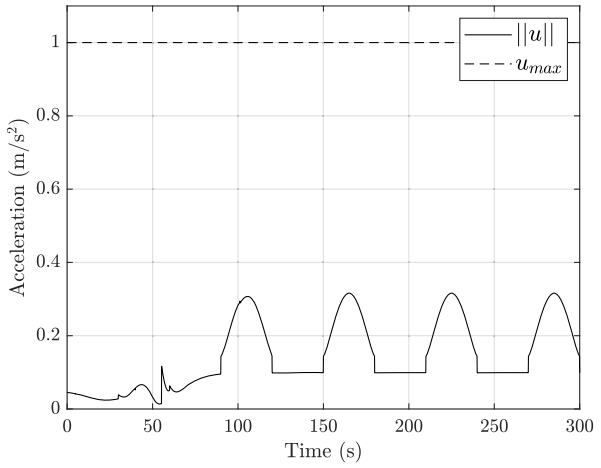

e) Acceleration norm over time - Case 3

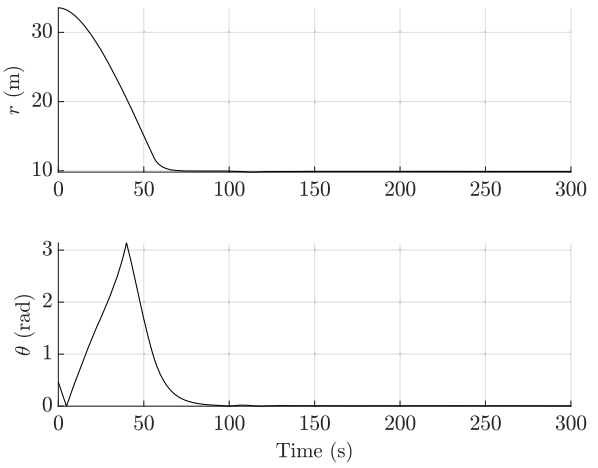

f) Convergence of r and θ over time - Case 3

Fig. 6 Maximum acceleration constraint: $u_{max} = 1.0$ m/s^2.

it is clear that the CLVF approach does not always use the full acceleration capabilities of the controlled vehicle. Rather, this approach designs the field such that under worst-case conditions the total acceleration commands can never rise above the constraints set by the vehicle. Sometimes, particularly good conditions will occur, and the chaser will use very little of the acceleration capabilities, such as in Fig. 6a. Unfortunately, it is possible that, in some design cases, there may be some small set of worst-case scenarios with quite high acceleration commands, but yet, a very low likelihood of occurring. In these particular cases, the current technique of finding an absolute bound results in an "overdesigned" field that very infrequently uses the full acceleration capabilities. Of course, an improved parameter selection procedure could likely circumvent this issue.

It should also be noted that, in certain cases, modest spikes in acceleration occurred while converging to the attractor (such a spike in acceleration is visible in the path of Fig. 8 as a relatively sharp turn at the attractor, and corresponds to the spike seen in Fig. 4a). This can be solved by including some penalty on jerk in the optimization that

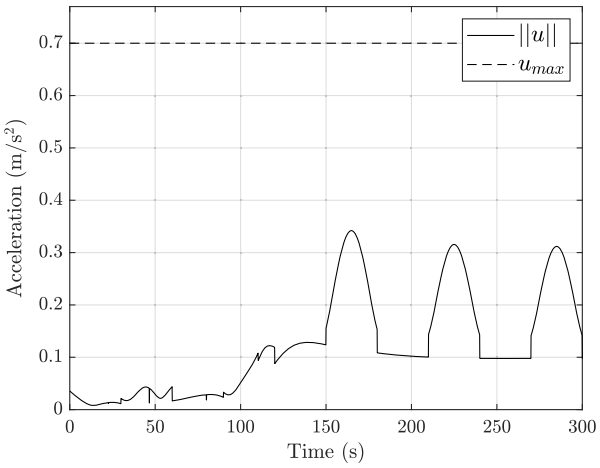

a) Acceleration norm over time - Case 1

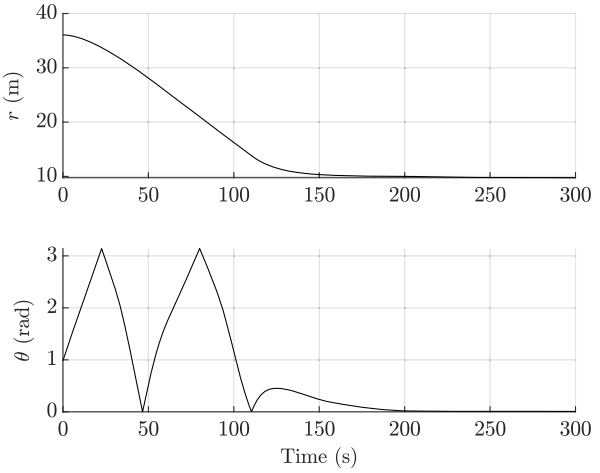

b) Convergence of r and θ over time - Case 1

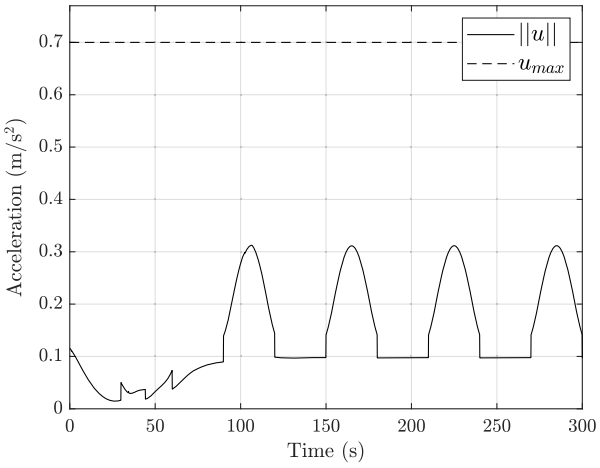

c) Acceleration norm over time - Case 2

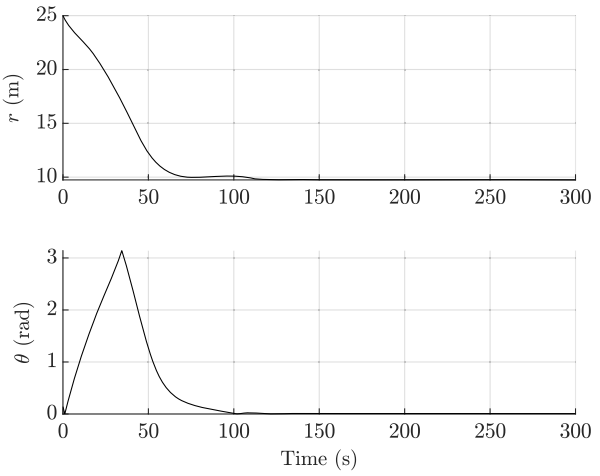

d) Convergence of r and θ over time - Case 2

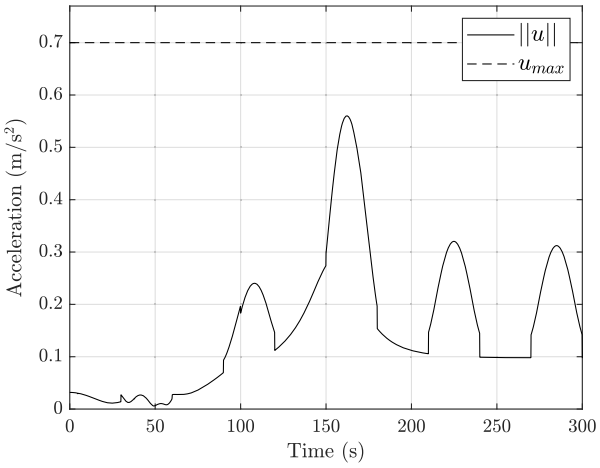

e) Acceleration norm over time - Case 3

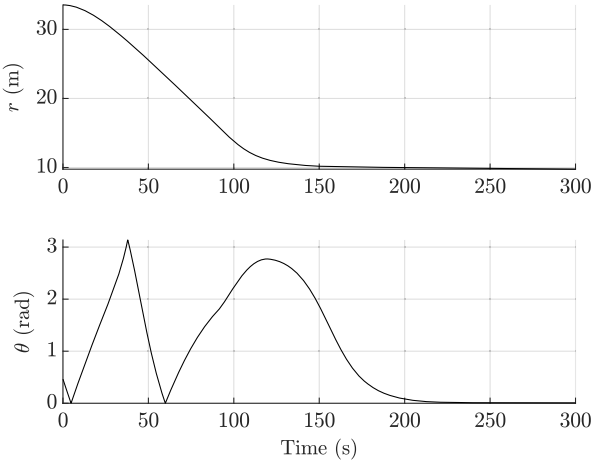

f) Convergence of r and θ over time - Case 3

Fig. 7 Maximum acceleration constraint: $u_{\max} = 0.70$ m/s^2.

solves for the field parameters k_c, k_a, and b. This would, of course, require a more sophisticated optimization compared to the line-search method, used in this work for simplicity.

VI. Conclusions

The cascaded Lyapunov vector field has been introduced to extend Lyapunov vector fields for use in spacecraft, with significant alterations to be suitable for use in generally rotating reference frames, and under acceleration constraints rather than velocity constraints.

A general stability analysis proved globally asymptotic stability given a set of conditions that are analogous to those of standard Lyapunov vector fields. Particular study of a special cascaded Lyapunov vector field with broadly applied assumptions such as a spherical attractor, a centered target, and velocity components that align with the Lyapunov function gradients was performed, and sufficient conditions to guarantee an upper acceleration bound were derived.

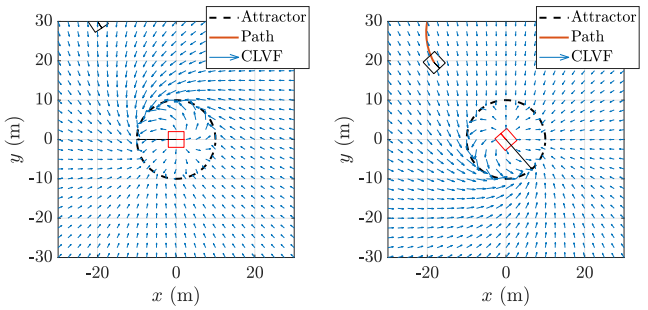

a) $t = 0.00$ s b) $t = 22.86$ s

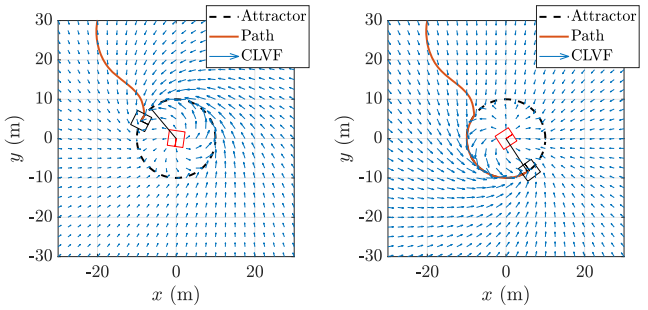

c) $t = 45.71$ s d) $t = 68.57$ s

Fig. 8 Time-lapse images of $u_{max} = 5.0$ m/s^2: case 1.

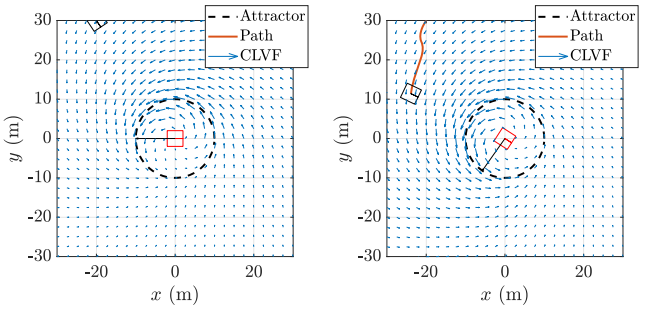

a) $t = 0.00$ s b) $t = 57.14$ s

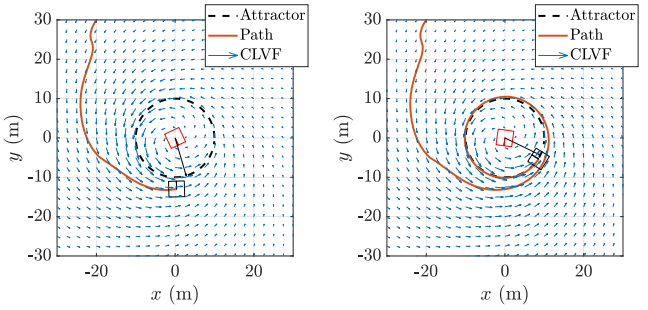

c) $t = 114.28$ s d) $t = 171.43$ s

Fig. 9 Time-lapse images of $u_{max} = 0.7$ m/s^2: case 1.

Furthermore, a particular design strategy for cascaded Lyapunov vector fields was developed, and an example of this design strategy was performed successfully for a spinning target spacecraft inspection mission. Simulations showed that the combined cascaded Lyapunov vector field guidance and control was successfully able to satisfy the path and acceleration constraints under various different acceleration capabilities and initial conditions. Importantly, these constraints were met without the use of any computationally heavy in-the-loop algorithms. It is also noteworthy that examples that include time-dependent trajectories within the attractor have been presented. While such trajectories are not prohibited by the general Lyapunov vector field theory, the authors are not aware of any cases where they have been used previously, and the inclusion of a second alignment field provides an explicit method for including time-dependent trajectories.

Acknowledgment

This work was financially supported in part by the Natural Sciences and Engineering Research Council of Canada under the Alexander Graham Bell Canada Graduate Scholarship Masters (CGSM 542715).

References

[1] Weiss, A., Baldwin, M., Erwin, R. S., and Kolmanovsky, I., "Model Predictive Control for Spacecraft Rendezvous and Docking: Strategies for Handling Constraints and Case Studies," *IEEE Transactions on Control Systems Technology*, Vol. 23, No. 4, 2015, pp. 1638–1647. https://doi.org/10.1109/TCST.2014.2379639

[2] Di Cairano, S., Park, H., and Kolmanovsky, I., "Model Predictive Control Approach for Guidance of Spacecraft Rendezvous and Proximity Maneuvering," *International Journal of Robust and Nonlinear Control*, Vol. 22, No. 12, 2012, pp. 1398–1427. https://doi.org/10.1002/rnc.2827

[3] Li, Q., Yuan, J., Zhang, B., and Gao, C., "Model Predictive Control for Autonomous Rendezvous and Docking with a Tumbling Target," *Aerospace Science and Technology*, Vol. 69, Oct. 2017, pp. 700–711. https://doi.org/10.1016/j.ast.2017.07.022

[4] Park, H., Zagaris, C., Virgili Llop, J., Zappulla, R., Kolmanovsky, I., and Romano, M., "Analysis and Experimentation of Model Predictive Control for Spacecraft Rendezvous and Proximity Operations with Multiple Obstacle Avoidance," *AIAA/AAS Astrodynamics Specialist Conference*, AIAA Paper 2016-5273, 2016. https://doi.org/10.2514/6.2016-5273

[5] Zhu, S., Sun, R., Wang, J., Wang, J., and Shao, X., "Robust Model Predictive Control for Multi-Step Short Range Spacecraft Rendezvous," *Advances in Space Research*, Vol. 62, No. 1, 2018, pp. 111–126. https://doi.org/10.1016/j.asr.2018.03.037

[6] Ventura, J., Ciarcia, M., Romano, M., and Walter, U., "An Inverse Dynamics-Based Trajectory Planner for Autonomous Docking to a Tumbling Target," *AIAA Guidance, Navigation, and Control Conference*, AIAA Paper 2016-0876, 2016. https://doi.org/10.2514/6.2016-0876

[7] Hough, J. G., and Ulrich, S., "Lyapunov Vector Fields for Thrust-Limited Spacecraft Docking with an Elliptically-Orbiting Uncooperative Tumbling Target," *AIAA Scitech 2020 Forum*, AIAA Paper 2020-2078, 2020. https://doi.org/10.2514/6.2020-2078

[8] Scorsoglio, A., and Furfaro, R., "ELM-based Actor-Critic Approach to Lyapunov Vector Fields Relative Motion Guidance in Near-Rectilinear Orbit," *2019 AAS/AIAA Astrodynamics Specialists Conference*, AIAA, Reston, VA, 2019, pp. 3767–3783.

[9] Lawrence, D., "Lyapunov Vector Fields for UAV Flock Coordination," *2nd AIAA "Unmanned Unlimited" Conference and Workshop & Exhibit*, AIAA Paper 2003-6575, 2003. https://doi.org/10.2514/6.2003-6575

[10] Lawrence, D. A., Frew, E. W., and Pisano, W. J., "Lyapunov Vector Fields for Autonomous Unmanned Aircraft Flight Control," *Journal of Guidance, Control, and Dynamics*, Vol. 31, No. 5, 2008, pp. 1220–1229. https://doi.org/10.2514/1.34896

[11] Frew, E. W., Lawrence, D. A., and Morris, S., "Coordinated Standoff Tracking of Moving Targets Using Lyapunov Guidance Vector Fields," *Journal of Guidance, Control, and Dynamics*, Vol. 31, No. 2, 2008, pp. 290–306. https://doi.org/10.2514/1.30507

[12] Pothen, A. A., and Ratnoo, A., "Curvature-Constrained Lyapunov Vector Field for Standoff Target Tracking," *Journal of Guidance, Control, and Dynamics*, Vol. 40, No. 10, 2017, pp. 2729–2736. https://doi.org/10.2514/1.G002281

[13] Sun, S., Wang, H., Liu, J., and He, Y., "Fast Lyapunov Vector Field Guidance for Standoff Target Tracking Based on Offline Search," *IEEE Access*, Vol. 7, Aug. 2019, pp. 124,797–124,808. https://doi.org/10.1109/ACCESS.2019.2932998

[14] Che, F., Niu, Y., Li, J., and Wu, L., "Cooperative Standoff Tracking of Moving Targets Using Modified Lyapunov Vector Field Guidance," *Applied Sciences*, Vol. 10, No. 11, 2020, p. 3709. https://doi.org/10.3390/app10113709

[15] Chen, H., Chang, K., and Agate, C. S., "UAV Path Planning with Tangent-Plus-Lyapunov Vector Field Guidance and Obstacle Avoidance," *IEEE Transactions on Aerospace and Electronic Systems*, Vol. 49, No. 2, 2013,

pp. 840–856.
https://doi.org/10.1109/TAES.2013.6494384
[16] Wilhelm, J. P., and Clem, G., "Vector Field UAV Guidance for Path Following and Obstacle Avoidance with Minimal Deviation," *Journal of Guidance, Control, and Dynamics*, Vol. 42, No. 8, 2019, pp. 1848–1856.
https://doi.org/10.2514/1.G004053
[17] Caveny, J., "On Integral Lipschitz Conditions and Integral Bounded Variation," *Journal of the London Mathematical Society*, Vol. s2-2, No. 2, 1970, pp. 346–352.
https://doi.org/10.1112/jlms/s2-2.2.346
[18] Boyd, S., and Vandenberghe, L., *Convex Optimization*, Cambridge Univ. Press, Cambridge, MA, 2004, Chap. 9, pp. 464–466.